AMERICAN SOCIETY FOR MICROBIOLOGY | Applied and Environmental Microbiology®

PLANT MICROBIOLOGY

Coordinated Regulation of the Size and Number of Polyhydroxybutyrate Granules by Core and Accessory Phasins in the Facultative Microsymbiont *Sinorhizobium fredii* NGR234

Yan-Wei Sun,[a,b,c] Yan Li,[d] Yue Hu,[a,b,c] Wen-Xin Chen,[a,b,c] Chang-Fu Tian[a,b,c]

[a]State Key Laboratory of Agrobiotechnology, College of Biological Sciences, China Agricultural University, Beijing, China
[b]MOA Key Laboratory of Soil Microbiology, College of Biological Sciences, China Agricultural University, Beijing, China
[c]Rhizobium Research Center, College of Biological Sciences, China Agricultural University, Beijing, China
[d]Key Laboratory of Coastal Biology and Utilization, Yantai Institute of Coastal Zone Research, Chinese Academy of Sciences, Yantai, China

ABSTRACT The exact roles of various granule-associated proteins (GAPs) of polyhydroxybutyrate (PHB) are poorly investigated, particularly for bacteria associated with plants. In this study, four structural GAPs, named phasins PhaP1 to PhaP4, were identified and demonstrated as true phasins colocalized with PHB granules in *Sinorhizobium fredii* NGR234, a facultative microsymbiont of *Vigna unguiculata* and many other legumes. The conserved PhaP2 dominated in regulation of granule size under both free-living and symbiotic conditions. PhaP1, another conserved phasin, made a higher contribution than accessory phasins PhaP4 and PhaP3 to PHB biosynthesis at stationary phase. PhaP3, with limited phyletic distribution on the symbiosis plasmid of *Sinorhizobium*, was more important than PhaP1 in regulating PHB biosynthesis in *V. unguiculata* nodules. Under the test conditions, no significant symbiotic defects were observed for mutants lacking individual or multiple *phaP* genes. The mutant lacking two PHB synthases showed impaired symbiotic performance, while mutations in individual PHB synthases or a PHB depolymerase yielded no symbiotic defects. This phenomenon is not related to either the number or size of PHB granules in test mutants within nodules. Distinct metabolic profiles and cocktail pools of GAPs of different *phaP* mutants imply that core and accessory phasins can be differentially involved in regulating other cellular processes in the facultative microsymbiont *S. fredii* NGR234.

IMPORTANCE Polyhydroxybutyrate (PHB) granules are a store of carbon and energy in bacteria and archaea and play an important role in stress adaptation. Recent studies have highlighted distinct roles of several granule-associated proteins (GAPs) in regulating the size, number, and localization of PHB granules in free-living bacteria, though our knowledge of the role of GAPs in bacteria associated with plants is still limited. Here we report distinct roles of core and accessory phasins associated with PHB granules of *Sinorhizobium fredii* NGR234, a broad-host-range microsymbiont of diverse legumes. Core phasins PhaP2 and PhaP1 are conserved major phasins in free-living cells. PhaP2 and accessory phasin PhaP3, encoded by an auxiliary gene on the symbiosis plasmid, are major phasins in nitrogen-fixing bacteroids in cowpea nodules. GAPs and metabolic profiles can vary in different *phaP* mutants. Contrasting symbiotic performances between mutants lacking PHB synthases, depolymerase, or phasins were revealed.

KEYWORDS PHB, legume, phasin, rhizobium, symbiosis

The metabolic ability to synthesize polyhydroxyalkanoates (PHAs), which are polyoxoesters of (*R*)-hydroxyalkanoic acid monomers, has been described for both bacteria and archaea (1). The most common PHA is poly(3-hydroxybutyrate) (PHB). High-molecular-weight PHB consisting of $>10^3$ 3-hydroxybutyrate residues is

Citation Sun Y-W, Li Y, Hu Y, Chen W-X, Tian C-F. 2019. Coordinated regulation of the size and number of polyhydroxybutyrate granules by core and accessory phasins in the facultative microsymbiont *Sinorhizobium fredii* NGR234. Appl Environ Microbiol 85:e00717-19. https://doi.org/10.1128/AEM.00717-19.

Editor Claire Vieille, Michigan State University

Address correspondence to Chang-Fu Tian, cftian@cau.edu.cn.

Received 27 March 2019
Accepted 23 July 2019
Accepted manuscript posted online 2 August 2019
Published 17 September 2019

present in the form of inclusion bodies (PHB granules) in prokaryote cells (2). The biosynthesis of PHB starts with the condensation of two molecules of acetyl coenzyme A (acetyl-CoA) by PhbA (3-ketothiolase) to give acetoacetyl-CoA, which is then reduced by PhbB (acetoacetyl-CoA reductase) to form 3-hydroxybutyryl-CoA. This compound is further polymerized to PHB by PhbC (PHB synthase). PHB degradation is initiated by PhaZ (PHB depolymerase) to release the 3-hydroxybutyrate monomer. PHB granules are accumulated under nutrient-limiting conditions (nitrogen, oxygen, phosphorus, etc.) but with an excess of carbon sources (1) and are considered a store of intracellular carbon and energy. Therefore, the PHB synthesis is tightly connected with the tricarboxylic acid (TCA) cycle, though the molecular mechanisms of acetyl-CoA partition between two processes remain elusive.

Beyond the storage function, the ability to accumulate PHB can enhance resistance of various bacteria, such as *Aeromonas hydrophila*, *Azospirillum brasilense*, *Escherichia coli*, *Methylobacterium extorquens*, and *Ralstonia eutropha*, to various stresses such as UV radiation, osmotic shock, hydroxyl radicals, and high or low temperatures (3–7). These protective roles of PHB have been considered a general phenomenon regardless of individual species or the type of stressing agent, but the underlying mechanisms are not well understood (8). The protective role of PHB is partially due to its hydrolysis product 3-hydroxybutyrate, which can act as a compatible solute protecting the activity of enzymes under osmotic and thermal stresses (9, 10). It was reported that methyl-esterified dimers and trimers of 3-hydroxybutyrate, produced by diverse bacteria during PHB degradation, have greater hydroxyl radical-scavenging activity than the monomer 3-hydroxybutyrate (6). Recent studies also show that a structural protein, PhaP, associated with PHB granules from *Azotobacter* sp. strain FA-8 has chaperone-like functions and stress-protecting effects in *E. coli* (11, 12). The *phaP* genes encode a group of low-molecular-weight proteins known as phasins, which are the major proteins surrounding the hydrophobic core of PHB granules. Other documented granule-associated proteins (GAPs) include PhbC, PhaZ, the transcriptional regulator of PHB synthesis PhaR, and some uncharacterized putative GAPs (13), while the suspected phospholipids in the surface layer are not found *in vivo* (14). The term carbonosome has been proposed for the complex organized subcellular structures of PHB granules surrounded by structural, biosynthetic, catabolic, and regulatory proteins (15). The importance of various GAPs has been highlighted by the distinct roles of several PhaPs and another GAP, PhaM, in the model strain *R. eutropha* H16. Among seven documented PhaPs, $PhaP1_{Reu}$ is the most abundant phasin in *R. eutropha* H16 and regulates the amount of PHB, as well as size and number of granules, while PhaM, which interacts with both PhbC and the nucleoid, is responsible for maximal activity of PHB synthase and subcellular localization of granules (16–18). These pioneering results suggest that the pool of GAPs and their putative roles during bacterial adaptations to fluctuating environmental conditions remain largely unexplored.

Rhizobia can form nitrogen-fixing nodules on legumes and play an important role in sustainable agriculture and the global nitrogen cycle. To reduce one molecule of N_2, 16 ATPs are required in the oxygen-sensitive nitrogen fixation process (19). Within nodule cells, rhizobia differentiate into nongrowing and nitrogen-fixing bacteroids that receive carbon and all the essential nutrients from the legume host (20). Low levels of free oxygen may limit the TCA cycle of bacteroids, possibly leading to the biased partition of acetyl-CoA to the biosynthesis of PHB (21). However, the accumulation level of PHB in bacteroids varies between different rhizobium-legume systems, such as with PHB granules present in *Glycine max* (soybean) nodules but not in *Medicago sativa* (alfalfa) nodules (22, 23). This contrasting feature could be partially due to variations in microenvironments of nodules from two legumes. This view is supported by the fact that bacteroids within nodules of soybean and alfalfa, respectively, are phosphate limited and nonlimited (24, 25). However, PHB granules became visible in bacteroids of the *phaZ* mutant of *Sinorhizobium meliloti* Rm1021 in alfalfa nodules (26), indicating simultaneously active biosynthesis and depolymerization of PHB in *S. meliloti* bacteroids in alfalfa. The symbiotic performance of the *phbC* mutant of various rhizobia

associated with corresponding legumes can be either defective (*S. meliloti* and *Azorhizobium caulinodans*) or enhanced (*Rhizobium etli*) (27–29). Our knowledge on GAPs of PHB in rhizobia is restricted to phasins of *S. meliloti* Rm1021 and *Bradyrhizobium diazoefficiens* USDA110 (27, 30, 31). Among the PhaPs differentially expressed in various culture media, $PhaP4_{Bdi}$ is the most abundant phasin in USDA110, and a $phaP1_{Bdi}$ $phaP4_{Bdi}$ double mutant formed a single, large cytoplasmic PHB granule (30, 31). $PhaP1_{Sme}$ and $PhaP2_{Sme}$ of Rm1021 may equally contribute to PHB production and symbiotic adaptation (27). Our previous transcriptomic analyses of *Sinorhizobium fredii* NGR234, characterized by its broad host range, revealed that three annotated phasin genes, *phaP1*, *phaP2*, and *phaP3*, exhibited distinct expression patterns within nodules of *Vigna unguiculata* and *Leucaena leucocephala* compared to those in free-living cultures (32), implying potential differentiated roles of these phasins under free-living and symbiotic conditions.

In this study, we aimed to characterize PhaP1, PhaP2, PhaP3, and other putative phasins of *S. fredii* NGR234 within nodules of *V. unguiculata* and under the nutrient-limiting conditions of the stationary phase. To this end, subcellular localizations of PhaPs and other representative GAPs, identified from proteomic analysis of purified PHB granules, were determined in wild-type NGR234 and *phbC* mutants. The number and size of PHB granules, and PHB amounts from individual and combined mutants of *phaP*s at stationary phase and within *V. unguiculata* nodules, were compared. Contrasting roles of different PhaPs in regulating granule size and number and PHB amounts under free-living and symbiotic conditions were revealed. These results were further discussed with the evidence of distinct metabolic profiles of *phaP* mutants, the pools of GAPs associated with representative mutants of *phaP*, and the contrasting phyletic distribution patterns of PhaPs in the genus *Sinorhizobium*.

RESULTS

Characterization of synthase and phasins of PHB in NGR234 at stationary phase. Within the genome of *S. fredii* NGR234, there are two genes, *phbC1* (*NGR_c34290*) and *phbC2* (*NGR_c14000*), encoding PHB synthase. In our exploratory experiments, a *phbC1 phbC2* (here referred to as *phbC1C2*) insertion mutant was constructed, and it had no PHB granules under free-living conditions. Then the Δ*phbC1*, Δ*phbC2*, and Δ*phbC1* Δ*phbC2* (here referred to as Δ*phbC1C2*) in-frame deletion mutants were constructed; these mutants had a growth rate similar to that of wild-type NGR234 in TY medium (see Materials and Methods) (Fig. 1A). The number of PHB granules at stationary phase was slightly reduced in the Δ*phbC1* mutant compared to that in the wild-type strain (Duncan's test, alpha = 0.05), while no granule could be observed in the Δ*phbC2* and Δ*phbC1C2* mutants (Fig. 1B and C). A genetic complementation experiment showed that the wild-type *phbC2* gene can restore the defects of the Δ*phbC1C2* mutant in forming PHB granules (Fig. 1B and C). In line with these observations from transmission electronic microscopy (TEM) pictures, PHB quantification experiments showed that PhbC2 was the major PHB synthase, while no significant difference in PHB content was observed among the Δ*phbC1* mutant, the Δ*phbC1C2* mutant complemented with *phbC2* (here referred to as Δ*phbC1C2*+*C2*), and NGR234 (see Table S1 in the supplemental material).

Three phasins were annotated in NGR234, i.e., PhaP1 (NGR_c03360), PhaP2 (NGR_c13240), and PhaP3 (NGR_a00900). Furthermore, the electrospray ionization mass spectrometry (ESI-MS) analyses described below led to the identification of a fourth putative phasin, PhaP4 (NGR_b11320). To test whether these putative phasins could be associated with PHB granules, PhaP1-enhanced yellow fluorescent protein (eYFP), PhaP2-eYFP, PhaP3-eYFP, and PhaP4-eYFP driven by a constitutively transcribed promoter were individually introduced into wild-type NGR234, the *phbC1C2* mutant (for eYFP fusions of PhaP1, PhaP2, and PhaP3), or the Δ*phbC1C2* mutant (for PhaP4-eYFP). The uniform fluorescence of the *phbC1C2* or Δ*phbC1C2* cells indicated soluble localization of free eYFP fused with PhaP1, PhaP2, PhaP3, or PhaP4 (Fig. 2A). In contrast, these

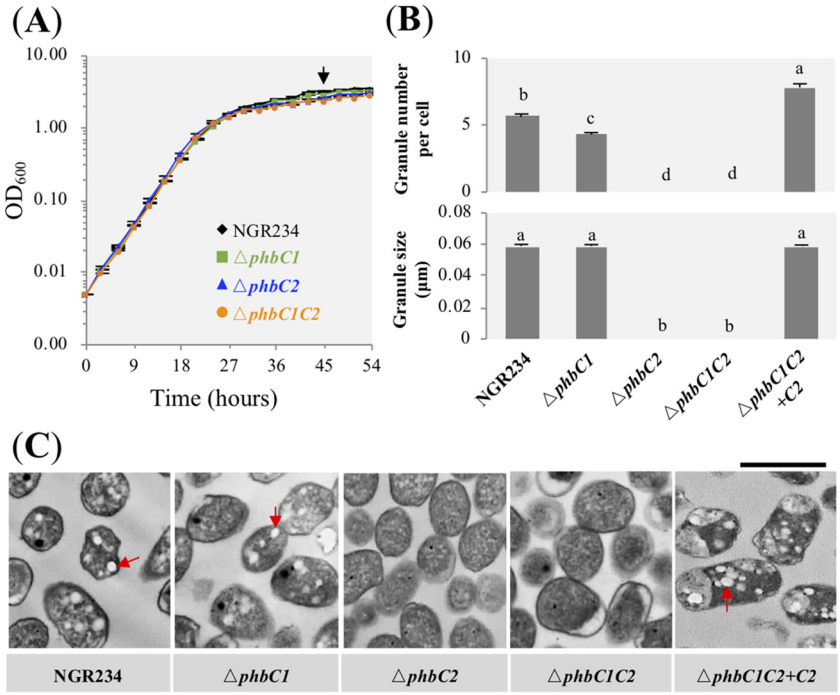

FIG 1 Characteristics of PHB granules in free-living NGR234 and mutants lacking PHB synthase. (A) Growth curves of test strains. Bacterial cells were collected at stationary phase, as indicated by an arrow. (B) Number and size of PHB granules. A total of 150 cells were scored for each strain. Values represent means ± SEMs. Different letters indicate significant difference (alpha = 0.05, Duncan's test). (C) Transmission electronic microscopy pictures. Red arrows indicate PHB granules. Bar, 1 μm.

phasin-eYFP fusions were colocalized with PHB granules, stained with Nile red in wild-type NGR234 (Fig. 2A).

Δ*phaP1*, Δ*phaP2*, Δ*phaP3*, and Δ*phaP4* in-frame deletion mutants and Δ*phaP1P2*, Δ*phaP1P3*, Δ*phaP2P3*, Δ*phaP1P4*, Δ*phaP2P4*, Δ*phaP3P4*, Δ*phaP1P2P3*, and Δ*phaP1P2P3P4* mutants were constructed. At stationary phase, the relative contributions to PHB synthesis decreased in the order from PhaP2, PhaP1, PhaP4, to PhaP3 according to PHB content detected in these 12 mutants (Table S1). The dominant role of PhaP2 at stationary phase was further supported by the fact that the largest PHB granule, around two times larger than that of the wild-type NGR234, was found in the Δ*phaP2* mutant (Duncan's test, alpha = 0.05). Among the double mutants, the Δ*phaP1P2* mutant synthesized the smallest amount of PHB (0.060 μg in 1 ml of bacterial culture with an optical density at 600 nm [OD_{600}] of 1.0), 8.6% to 19.4% of the PHB content in the other five double mutants (Table S1). Although a few PHB granules can be observed in TEM pictures of the Δ*phaP1P2* mutant, the amount of PHB in the Δ*phaP1P2* mutant was not significantly different from that of the Δ*phaP1P2P3* or Δ*phaP1P2P3P4* mutant, for which no PHB granule was found in test TEM pictures (Fig. 2B and C and Table S1). Therefore, PhaP3 and PhaP4 had relatively minor roles in regulating the biosynthesis of PHB granules at stationary phase. The difference in the numbers of PHB granules among test mutants except the Δ*phaP1P2P3* and Δ*phaP1P2P3P4* mutants can be more than 10 times, with the average granule number below 0.40 in the Δ*phaP1P2* mutant and 4.46 granules in the Δ*phaP1* mutant (Fig. 2B). This was supported by PHB quantification results (Table S1). Notably, these numbers of granules and PHB amounts in test phasin mutants were lower than for NGR234 in different degrees (Fig. 2B and Table S1), suggesting cumulative contributions by the four phasins.

Role of phasins and PHB synthase in the symbiosis with *V. unguiculata*. Sequence analysis demonstrated that PhaP1 and PhaP2 are highly conserved phasins encoded by core genes on chromosomes of *Sinorhizobium*, while PhaP4 and PhaP3 are restricted to a subset of species/strains, i.e., are encoded by accessory genes (Fig. 3A).

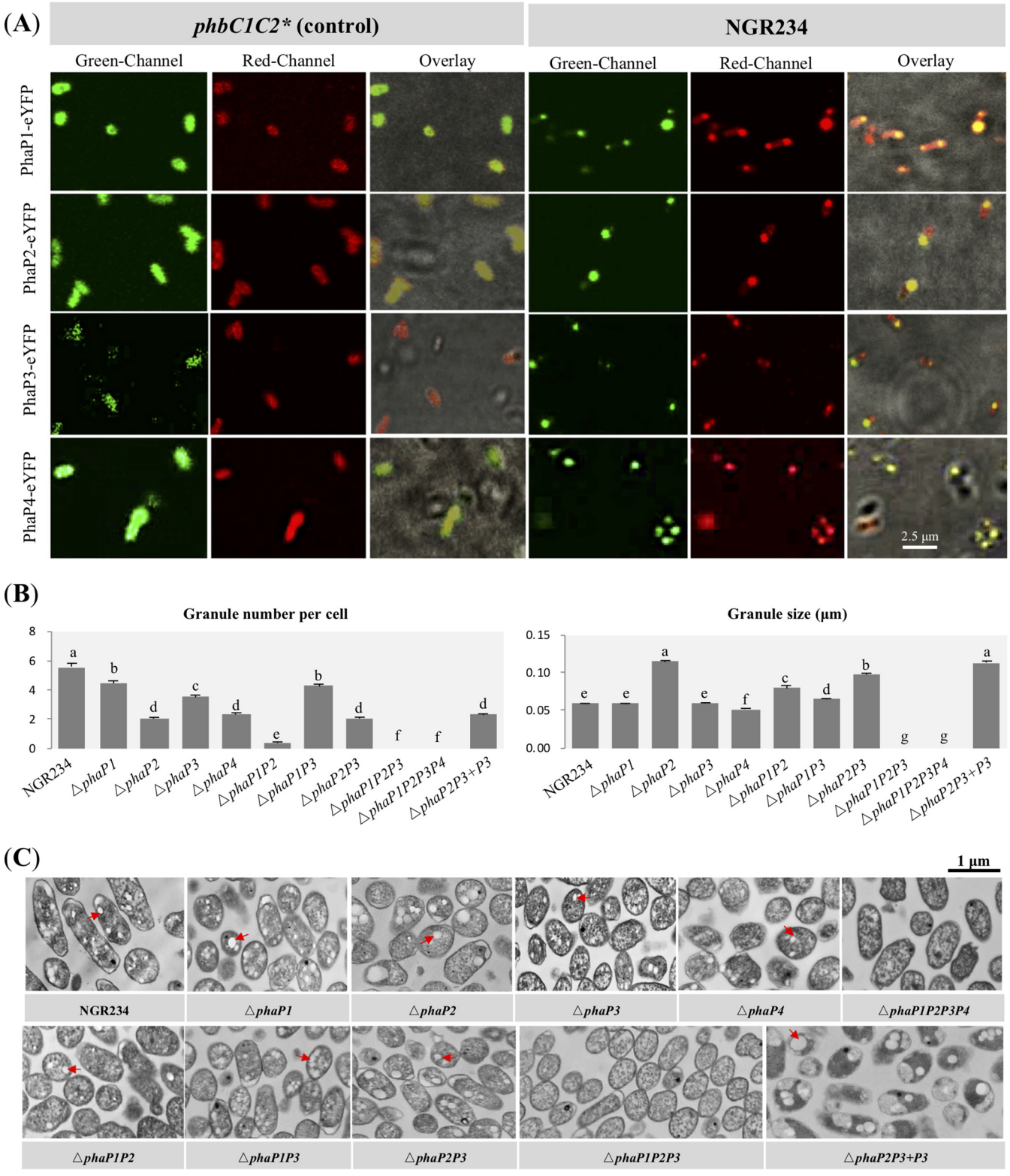

FIG 2 Characteristics of PHB granules in free-living NGR234 and mutant strains lacking genes encoding phasins. (A) Subcellular colocalization of predicted phasins with PHB granules. PhaP1-eYFP, PhaP2-eYFP, PhaP3-eYFP, and PhaP4-eYFP fusions were constitutively expressed in free-living NGR234 and its *phbC1C2* mutant (*, Δ*phbC1C2* used for expressing PhaP4-eYFP). The *phbC1C2* (or Δ*phbC1C2*) mutant served as a control with no PHB accumulation. Fluorescence microscopic images were generated after staining with Nile red in the red channel (indicating the localization of PHB granules) or without staining in the green channel (showing the localization of phasins). (B) Number of PHB granules within each bacterial cell and size of PHB granules. A total of 150 cells were scored for each strain (58 cells were scored for the Δ*phaP1P2* mutant; these values were obtained under the same conditions as for Fig. 1, and the same values for NGR234 were used in this case). Values represent means ± SEMs. Different letters indicate significant difference (alpha = 0.05, Duncan's test). (C) Transmission electronic microscopy pictures of bacterial cells at stationary phase. Red arrows indicate PHB granules. Bar, 1 μm.

The *phaP4* homologs were found in chromids of *Sinorhizobium* sp. strain CCBAU05631 and all analyzed *S. fredii* strains except USDA257. A *phaP4* homolog in USDA257 is located in a chromosomal region of 2 Mb displaying similarity to chromids of other *S. fredii* strains (33, 34). The *phaP3* homologs were present in the symbiosis plasmid of *Sinorhizobium* sp. CCBAU05631 and *S. fredii* CCBAU83666 and NGR234. Mutants lacking individual or multiple phasin-coding genes were inoculated on *V. unguiculata* (Fig. 3B); little variation in leaf chlorophyll content and shoot dry weight was found among plants inoculated with these strains under the test conditions (Table S2). All of these phasin deletion mutants formed pink nodules (Fig. 3C). Similar to the case with free-living cells, PhaP2 played a dominant role in regulating PHB granule size in nodules (Fig. 3B and C). In contrast to its minor role in regulating PHB synthesis in stationary-phase cultures, PhaP3 seemed to have a greater role in PHB biosynthesis than PhaP1 in nodules, as the PHB content of the Δ*phaP3* mutant was only half of that detected in the Δ*phaP1* mutant or NGR234 (Table S1). Moreover, Δ*phaP2P3* and Δ*phaP3P4* bacteroids harbored 32.6% and 42.6% of the PHB content detected in the Δ*phaP1P2* and Δ*phaP1P4* mutants, respectively (Table S1). This was also supported by the number of PHB granules observed in representative TEM pictures of bacteroids (Fig. 3B and C). This is in line with the strong upregulation of the *phaP3* gene in *V. unguiculata* nodules (32). A genetic complementation experiment showed that the wild-type *phaP3* gene can significantly increase the granule number and PHB content in the Δ*phaP2P3* mutant in nodules but not in stationary-phase culture (Fig. 2B and 3B and Table S1). Therefore, *phaP3* located in symbiosis plasmid plays a greater role in regulating the number of PHB granules under symbiotic condition than in free-living culture. Although individual mutants of *phaP1* and *phaP4* had little defects in the number or size of PHB granules in bacteroids (Fig. 3B and C), PHB quantification results for various double mutants, as well as for the Δ*phaP1P2P3* and Δ*phaP1P2P3P4* mutants, suggest that PhaP1 and PhaP4 make a cumulative contribution to PHB biosynthesis in bacteroids (Table S1).

In bacteroids from *V. unguiculata* nodules induced by mutants lacking PHB synthase, PHB granules were barely found for the Δ*phbC2* and Δ*phbC1C2* mutants (Fig. 4A), and bacteroids of these two mutants harbored less than 17% of the PHB content detected in wild-type NGR234 (Table S1). A significant increase of granule number was observed for the *NGR_b03370* mutant lacking a putative PHB depolymerase (PhaZ) compared to that for wild-type NGR234 (12.32 $\pm$ 0.80 versus 7.52 $\pm$ 0.50 per cell, average $\pm$ standard error of the mean [SEM]; Duncan's test, alpha $=$ 0.05 [Fig. 4B]). The average size of PHB granules was slightly but significantly larger in this *phaZ* (*NGR_b03370*) mutant than that of wild-type NGR234 (0.08 $\pm$ 0.002 versus 0.064 $\pm$ 0.002, average $\pm$ SEM; Duncan's test, alpha $=$ 0.05). All of these mutants formed pink nodules (Fig. 4A), and the inoculated plants were indistinguishable from each other regarding the chlorophyll content of leaf (Table S2), though a significant decrease of shoot dry weight was observed for the plants inoculated with the Δ*phbC1C2* mutant (Table S2; Kruskal-Wallis test followed by Mann-Whitney test with Bonferroni correction). This symbiotic defect and PHB biosynthesis of the Δ*phbC1C2* mutant can be restored by complementation using the wild-type *phbC2* gene (Table S2 and Fig. 4). Moreover, the Δ*phbC1C2* mutant occupied only 25.2% of *V. unguiculata* nodules in the presence of an equal amount of wild-type NGR234 cells ($P < 0.05$ [Fig. S2]).

Cocktail proteins associated with PHB granules in NGR234. Among four phasins, the in-frame deletion of *phaP2* caused the most dramatic change in the size of PHB granules (Fig. 2B). It has been reported on the basis of our previous transcriptome sequencing (RNA-seq) analysis (32) that *phaP2* was constitutively transcribed under both free-living and symbiotic conditions, while *phaP1* and *phaP3* were down- and upregulated, respectively, in *V. unguiculata* nodules. The *phaP4* gene was also upregulated in nodules, though to a lesser extent than *phaP3* (32). In this study, we further investigated whether the change of granule size in the Δ*phaP2* mutant would lead to a shift of the abundance and/or diversity of proteins associated with PHB granules. The Δ*phaP1* and Δ*phaP1P2* mutants were also included for comparison. PHB granules and

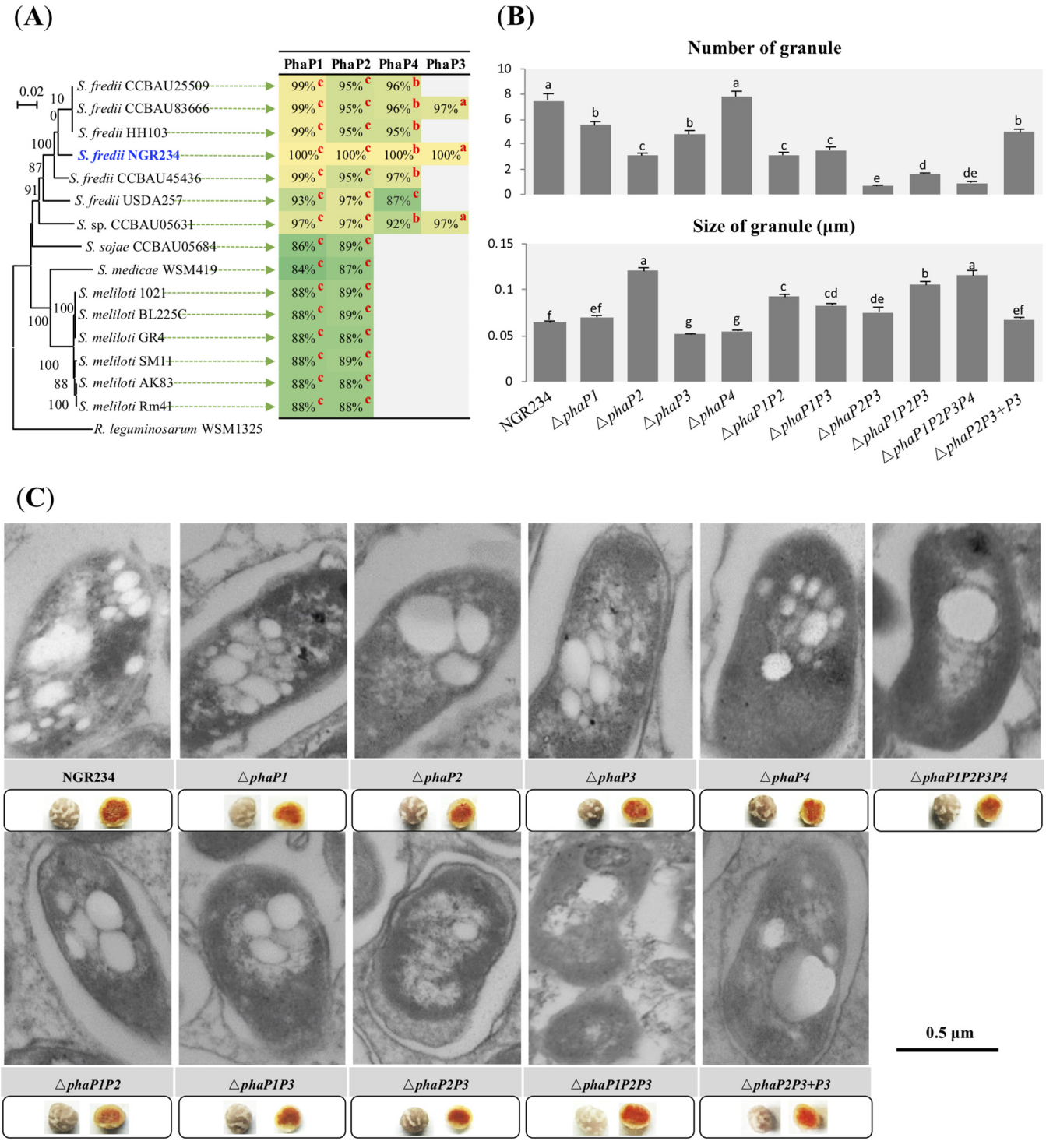

FIG 3 Characteristics of PHB granules in bacteroids of NGR234 and mutant strains lacking genes encoding phasins. (A) Neighbor-joining phylogenetic tree of the *rpoB* gene and phyletic distribution of PhaP1 to PhaP4 in *Sinorhizobium*. Identity values of homologs of PhaPs (query coverage above 60%) in corresponding genomes are shown. Superscript c, b, and a represent genome locations of homologous *phaP* genes on the chromosome, chromid, and symbiosis plasmid, respectively. The background colors were scaled from the minimum similarity value of 84% (green) to 100% (yellow). (B) Number of PHB granules within each bacterial cell and size of PHB granules. Seventy-five bacterial cells (mutants) or 50 bacterial cells (wild-type NGR234) were scored. Values represent means ± SEMs. Significant difference between means is indicated by different letters based on Duncan's test (alpha = 0.05). (C) Pictures of ultrathin sections of nodules obtained under transmission electronic microscopy. Pictures of more bacterial cells are shown in Fig. S1.

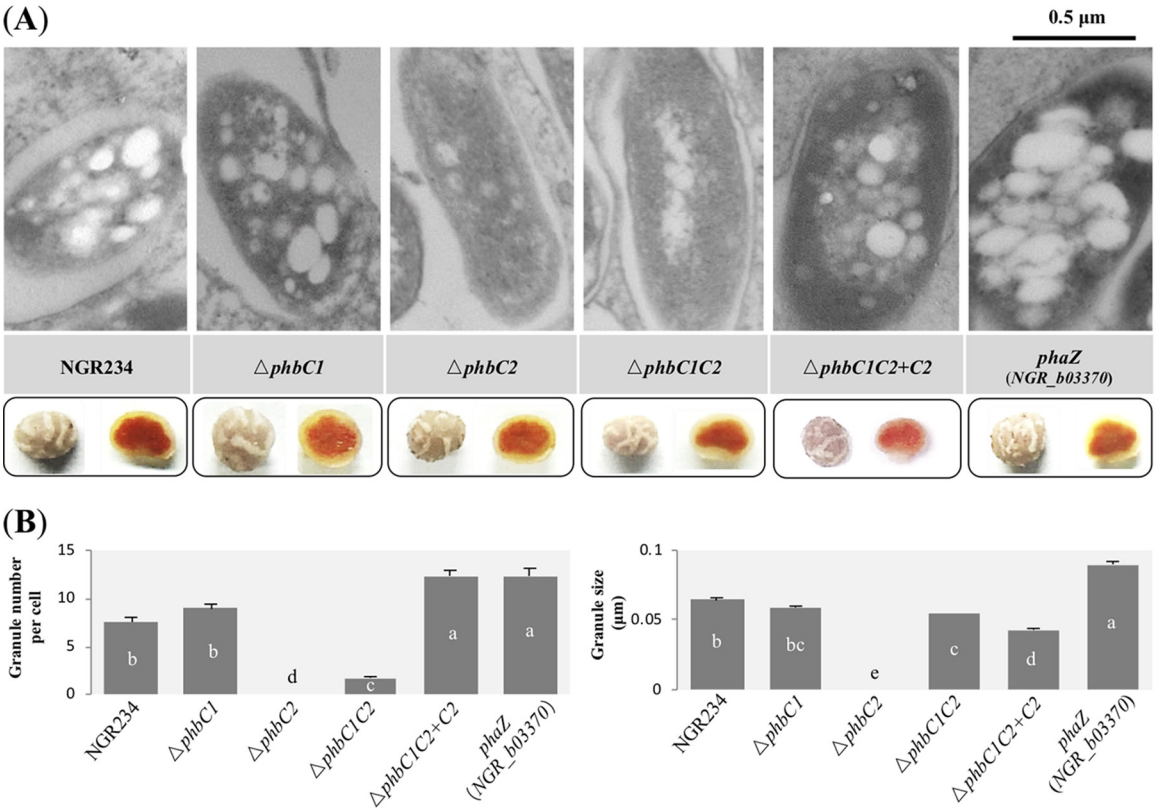

FIG 4 Characteristics of PHB granules in bacteroids of NGR234 and mutant strains lacking genes encoding PHB synthases or PHB depolymerase. (A) Pictures of ultrathin sections of nodules obtained under transmission electronic microscopy. Pictures of intact nodules and nodule halves are shown. Pictures of more bacterial cells are shown in Fig. S1. (B) Number of PHB granules within each bacterial cell and average size of PHB granules. Seventy-five bacterial cells (mutants) or 50 bacterial cells (wild-type NGR234) were scored. Values represent means ±SEMs. Significant difference between means is indicated by different letters based on Duncan's test (alpha = 0.05).

associated proteins (Fig. S3A) were enriched as described in Materials and Methods for stationary-phase cultures. The enriched PHB-associated proteins compared to crude proteins of bacteria at stationary phase could be observed in SDS-PAGE for NGR234 (Fig. S3B). There was also notable variation in electrophoresis patterns for PHB granule-associated proteins (GAPs) from the Δ*phaP1*, Δ*phaP2*, and Δ*phaP1P2* mutants (Fig. S3C). Bands corresponding to PhaP1, PhaP2, and PhaP4 were identified by MS analysis (Fig. S3B and S3C), confirming the reliability of test mutants. The nanospray ESI-MS analysis was used to identify proteins associated with PHB granules (Fig. 5A; a complete list of significant hits of $P < 0.05$ for each strain in three independent experiments is shown in Data Set S1). In wild-type NGR234 and the Δ*phaP1* mutant, PhaP2 was the most abundant protein associated with PHB granules. PhaP1 was the most abundant GAP in the Δ*phaP2* mutant. A conserved hypothetical protein, NGR_b11320, was found to be the most abundant GAP in the Δ*phaP1P2* mutant and could be found in NGR234 and the Δ*phaP1* and Δ*phaP2* mutants. Further sequence analysis revealed that it contains a Phasin_2 domain (Pfam family PF09361), which is also present in PhaP1, PhaP2, and PhaP3. NGR_b11320 was named PhaP4 accordingly.

In contrast to typical phasins (PhaP1, PhaP2, and PhaP4), other putative GAPs identified in this study had lower abundances (Fig. 5B), such as cytochrome *c* oxidase FixO2 (NGR_c17980), ATP synthase subunit beta (NGR_c31110), NADH-quinone oxidoreductase chain C NuoC (NGR_c10500), and a putative universal stress protein (NGR_c09750) detected in all test strains. PHB granules from the Δ*phaP1*, Δ*phaP2*, and Δ*phaP1P2* mutants seemed to have a relatively higher abundance than those from NGR234 in a hypothetical protein (NGR_b13620), ATP synthase subunit alpha (NGR_c31130), and polyhydroxyalkanoate synthesis repressor PhaR (NGR_c32730). No-

(A)

emPAI: 100 50 25 10 5

Gene	Functions	NGR234	Δ*phaP1*	Δ*phaP2*	Δ*phaP1P2*	pSORTb	COG
NGR_c13240	hypothetical protein (PhaP2)	3663.58	13695.92	4.16	6.18	Unknown	S
NGR_b11320	conserved hypothetical protein (PhaP4)	84.69	197.07	111.95	84.93	Unknown	S
NGR_c03360	hypothetical protein (PhaP1)	83.66	5.23	524.09	5.23	Unknown	S
NGR_c31110	ATP synthase subunit beta	13.67	11.56	17.56	22.64	Cyto [M]	C
NGR_c17980	cytochrome-c oxidase (FixO2)	17.43	17.47	17.4	14.84	Cyto	C
NGR_c09750	putative universal stress protein	15.42	11.43	11.39	11.43	Cyto	T
NGR_c10500	NADH-quinone oxidoreductase chain C (NuoC)	9.5	9.52	11.57	11.61	Cyto	C
NGR_b13620	hypothetical protein	7.04	9.46	13.24	17.56	Cyto	S
NGR_c31130	ATP synthase subunit alpha	6.39	9.08	13.75	11.69	Cyto	C
NGR_c32730	polyhydroxyalkanoate synthesis repressor (PhaR)	5.74	8.89	10.93	36.65	Cyto	S
NGR_c03840	hypothetical protein	0.76	2.1	38.49	44.73	Peri	S
NGR_c33940	ATP dependent phosphoenolpyruvate carboxykinase	3.23	5.54	15.64	16.97	Cyto	C
NGR_c17970	cytochrome-c oxidase (FixP2)	7.8	6.7	14.14	12.26	Peri	C
NGR_c04500	Fo ATP synthase B chain	4.3	1.05	12.74	16.5	Unknown	C
NGR_c26300	glutathione-independent formaldehyde dehydrogenase	6.36	6.37	13.77	6.37	Cyto	C
NGR_c31350	succinate dehydrogenase flavoprotein subunit	5.58	5.59	12.11	6.96	CM	C
NGR_c14000	poly-beta-hydroxybutyrate polymerase (PhbC2)	0.64	0.45	9.33	5.34	Cyto	I
NGR_c25180	putative ATP-binding component of ABC transporter	6.83	6.84	9.12	6.84	CM	E
NGR_c28710	molecular chaperone small heat shock protein	5.81	5.82	7.65	27.79	Cyto	O
NGR_c36120	putative outer membrane protein	1.96	2.55	4.09	17.11	OM	M
NGR_b18390	UTP--glucose-1-phosphate uridylyltransferase	1.77	1.44	5.75	15.51	Cyto	M
NGR_c21410	oxidoreductase	3.73	7.21	8.83	10.84	Cyto	E
NGR_c10510	NADH dehydrogenase I chain D (NuoD)	1.55	3.07	7.57	10.38	Cyto [M]	C
NGR_c29020	sarcosine oxidase, alpha subunit (SoxA)	3.25	3.79	7.59	9.48	Cyto	E
NGR_c33730	polyhydroxyalkanoate depolymerase	3.08	3.46	4.79	9.75	Cyto	I
NGR_b13770	ABC oligopeptide transporter, fused ATPase subunits	4.34	4.35	6.14	9.31	CM	S
NGR_c28100	fructose-bisphosphate aldolase	7.62	5.88	8.65	8.68	Cyto	G
NGR_c14720	putative invasion-associated protein	2.66	3.41	8.23	3.41	Unknown	S
NGR_c13410	group 1 outer membrane protein precursor	4.24	4.25	5.09	7.68	OM	M
NGR_c10560	NADH dehydrogenase I chain G (NuoG)	7.06	7.55	6.61	5.82	Cyto [M]	C
NGR_c15510	hypothetical protein	5.24	3.9	6.96	3.9	Unknown [M]	S
NGR_b19610	septum site-determining protein	8.86	6.42	10.36	8.88	Cyto	D

(B)

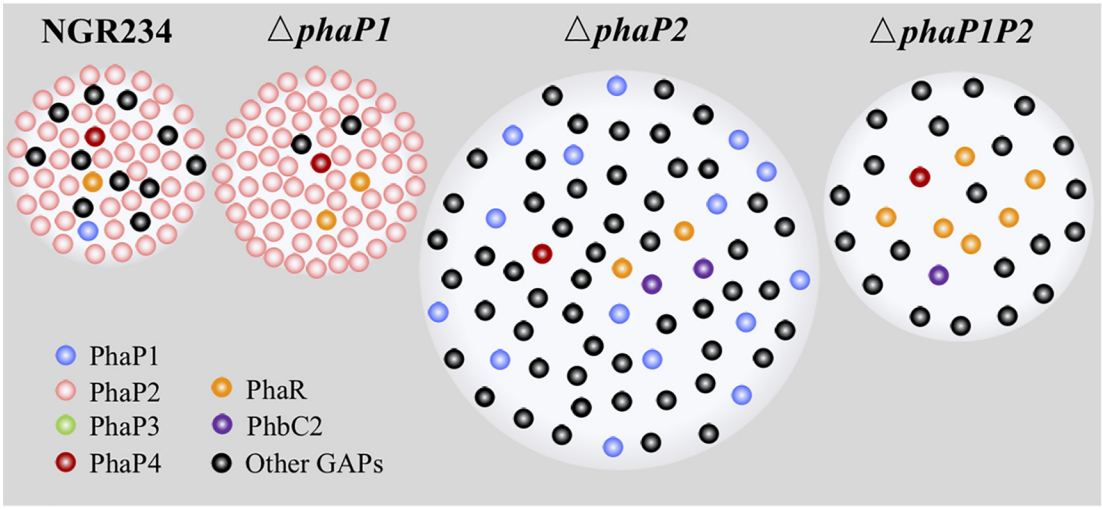

FIG 5 PHB granule-associated proteins from NGR234 and strains lacking *phaP1* and/or *phaP2*. (A) Exponentially modified protein abundance index (emPAI) for PHB granule-associated proteins (GAPs) identified using nanospray ESI-MS analysis. GAPs with a protein score above 1,500 (except NGR_b19610, serving as a control for a GAP with a protein score below 1,500 in the following colocalization experiment) in at least one test strain and identified from at least two out of three independent experiments (Data Set S1) are shown (emPAI values from the first experiment are shown). Subcellular localization predicted by pSORTb is shown as follows: OM, outer membrane; CM, cytoplasmic membrane; Cyto, cytoplasmic; Peri, periplasmic; superscript M, the protein may have multiple localization sites. The COG category of each protein is listed as follows: S (function unknown), C (energy production and conversion), T (signal transduction mechanism), I (lipid transport and metabolism), E (amino acid transport and metabolism), M (cell wall/membrane/envelope biogenesis), O (posttranslational modification, protein turnover, and chaperones), and G (carbohydrate transport and metabolism). (B) Schematic view of PHB granules and GAPs at stationary phase. The sizes of PHB granules in each strain are proportional to those average sizes determined for Fig. 2. The granule surface was largely occupied by PhaPs in NGR234 and the Δ*phaP1* and Δ*phaP2* mutants. The abundance of the regulator PhaR and the total pool of other GAPs excluding PhaPs increased in the Δ*phaP1P2* mutant.

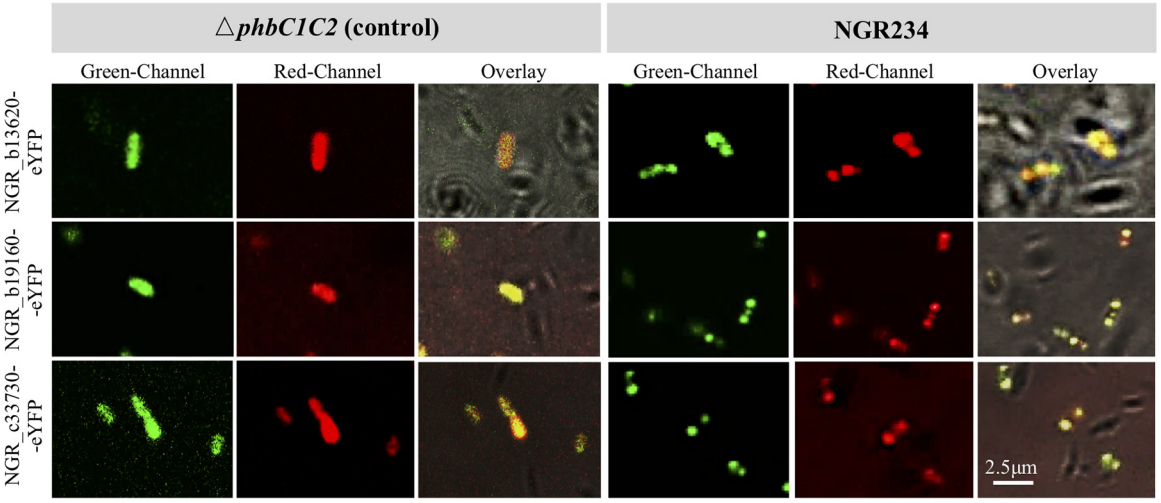

FIG 6 Subcellular colocalization of representative granule-associated proteins of low abundance. NGR_b13620-eYFP, NGR_b19160-eYFP, and NGR_c33730-eYFP fusions were constitutively expressed in free-living NGR234 and its Δ*phbC1C2* mutant.

tably, the abundance of PhaR was particularly higher in the Δ*phaP1P2* mutant than the other test strains. Similarly, PHB granules from the Δ*phaP2* and Δ*phaP1P2* mutants had a higher abundance in a hypothetical protein (NGR_c03840) and ATP-dependent phosphoenolpyruvate carboxykinase (NGR_c33940). Several proteins with a relatively high abundance in either the Δ*phaP2* or Δ*phaP1P2* mutant were also identified, such as a formaldehyde dehydrogenase (NGR_c26300), a succinate dehydrogenase flavoprotein subunit (NGR_c31350), and PhbC2 (NGR_c14000) in the Δ*phaP2* mutant and NGR_c28710 (a small heat shock protein), NGR_c36120 (a putative outer membrane protein), and NGR_b18390 (a uridylyltransferase) in the Δ*phaP1P2* mutant. Among these putative GAPs, the most abundant ones belong to the Clusters of Orthologous Groups (COG) categories S (function unknown), C (energy production and conversion) and T (signal transduction mechanism). A schematic overview of relative abundances of these GAPs in test strains at stationary phase is shown in Fig. 5B.

In addition to PhaP4 (NGR_b11320) (Fig. 2A), three representative GAPs of low abundances (NGR_b13620, NGR_c33730, NGR_b19610) (Fig. 5A and Data Set S1) were individually fused with the eYFP reporter and introduced into the Δ*phbC1C2* mutant and NGR234. These constitutively expressed proteins were colocalized with PHB granules in NGR234 while having a uniform intracellular distribution in the Δ*phbC1C2* mutant (Fig. 6).

Metabolic characteristics of NGR234 and its derived mutants. As described above, no direct relationship could be established between the number or size of PHB granules and the symbiotic performance of test mutants of genes involved in biosynthesis, depolymerization, and regulation of granule size and number. A Biolog GEN III plate was further used to compare the potential differences between these strains in their metabolic characteristics (Table S3). The Δ*phaP1P2* mutant was impaired in utilizing L-alanine, L-lactic acid, propionic acid, D-fructose-6-phosphate, and glycyl-L-proline. The Δ*phaP2P3* mutant exhibited reduced growth on acetoacetic acid, L-lactic acid, D-malic acid, and glycyl-L-proline. However, the Δ*phaP1P2P3* grew better than the Δ*phaP1P2* or Δ*phaP2P3* mutant on L-alanine or acetoacetic acid. Similarly, the Δ*phaP1P2P3P4* mutant and other mutants lacking individual or multiple phasins had their own characteristic metabolic profiles (Table S3). The Δ*phbC1C2* mutant was distinct by its improved utilization of diverse nutrients compared to wild-type NGR234 and Δ*phbC1*, Δ*phbC2*, *phaZ*, and phasin mutants (Table S3).

DISCUSSION

PHB synthase is involved in effective symbiosis. PHB granules could rarely be observed in the Δ*phbC2* and the Δ*phbC1C2* mutants of *S. fredii* NGR234 under both

free-living and symbiotic conditions. This is consistent with the absence of PHB granules in the free-living *phbC* mutant of *S. meliloti* Rm1021 (27). *Medicago truncatula* or *M. sativa* plants inoculated with the *phbC* mutant of *S. meliloti* showed reduced shoot dry weight and competition in nodule occupancy (23, 27, 35). In this study, reduced shoot dry weight of *V. unguiculata* was observed when this plant was inoculated with the Δ*phbC1C2* mutant rather than the mutant lacking a single PHB synthase. In contrast to the actively transcribed *phbC2* of NGR234 under both free-living and symbiotic conditions, upregulation of *phbC1* in nodules of *V. unguiculata* compared to free-living cultures was observed in our previous transcriptomic analyses (32). Moreover, the Δ*phbC1C2* mutant exhibited a more drastic change from wild-type NGR234 in metabolic profiles than the Δ*phbC2* or Δ*phbC1* mutant did. All test strains in this study were able to use L-aspartate and L-malate, while the Δ*phbC1C2* mutant showed enhanced ability to use D-aspartate and D-malate. Although less abundant in nature than L-amino acids, D-amino acids, including D-aspartate, have been detected and play diverse roles in plants, bacteria, and animals (36, 37). Transport and oxidization of D-malate into pyruvate by *E. coli* have been demonstrated (38). The Δ*phbC1C2* mutant also exhibited increased metabolism of citrate. These metabolic profiles of the Δ*phbC1C2* mutant indicated an upshift of the TCA cycle, which may be limited by the low-oxygen condition of infected nodule cells harboring nitrogen-fixing rhizobia (21). The downregulation of the TCA cycle in bacteroids is also supported by comparative transcriptomics of wild-type NGR234 in free-living culture and *V. unguiculata* nodules (32), where bacteroids exhibited reduced transcript levels of the genes encoding isocitrate dehydrogenase (NGR_c16430), α-ketoglutarate dehydrogenase E1 and E2 components (NGR_c31270 and NGR_c31260), and the catalytic subcomplex (SdhA/B, encoded by *NGR_c31350* and *NGR_c31340*, respectively) of succinate dehydrogenase.

It is notable that there was a low number of PHB granules in the Δ*phbC1C2* mutant in *V. unguiculata* nodules, whereas no PHB granules were found in a free-living culture of this mutant. Potential false positives could not be ruled out due to potential cytoplasmic changes in this mutant. This could be partially supported by PHB quantification results (Table S1) showing that no significant difference between the Δ*phbC1C2* and Δ*phbC2* mutants could be detected under both free-living and symbiotic conditions, though average PHB amounts were higher in nodules infected by the Δ*phbC1C2* mutant than by the Δ*phbC2* mutant. Alternatively, other proteins of similar function might exert a complementary effect to a limited extent. For example, NGR_b13620 shown as a putative GAP (Fig. 6) has a conserved domain (DUF3141), which shows a significant (E value, 2e−05) but low identity (23%) to poly(*R*)-hydroxyalkanoic acid synthase, class III PhaC subunit (WP_012267458.1). It is also annotated as 3-hydroxyalkanoate synthetase in many bacteria. Moreover, this gene is strongly induced in bacteroids in *V. unguiculata* nodules compared to free-living culture ($\log_2 R = 7.16$) (32). It has been reported that a *phbC* mutant of *S. meliloti* was unable to utilize acetoacetate, which is an intermediate in the degradation portion of the PHB cycle (39). The Δ*phbC1* mutant rather than the Δ*phbC1C2* or Δ*phbC2* mutant of NGR234 showed impaired ability in acetoacetate utilization (Table S3). These findings imply that the differential regulation and diversity of enzymes involved in PHB cycle in different species may contribute to their distinct adaptation characteristics.

As shown by ESI-MS and colocalization experiments, there is another putative PHB depolymerase (NGR_c33730) that shows poor identity (9.16%) to NGR_b03370 in NGR234. Sequence alignment with a PHA depolymerase database (40) suggested that NGR_c33730 and NGR_b03370 might belong to intracellular (i-nPHAscl, no lipase box) and extracellular (e-dPHAscl, catalytic domain type 1, with lipase box GLSAG) depolymerase families, respectively. However, there was evidence that an extracellular PHAscl depolymerase from *Paucimonas lemoignei* only degrades native PHA granules (41). Although *NGR_b03370* was transcribed at a relatively lower level than *NGR_c33730* in free-living culture, it was more strongly upregulated in *V. unguiculata* nodules (32) and the *phaZ* (*NGR_b03370*) mutant in nodule cells harbored more PHB granules of larger size than the wild-type NGR234. Visible PHB granules in bacteroids were observed for

the *phaZ* mutant but not wild-type Rm1021 of *S. meliloti* in *Medicago* nodules (26). However, these *phaZ* mutants of NGR234 and Rm1021 were indistinguishable from wild-type strains in symbiotic performance in this study and the earlier one (26). This is in line with the view that degradation of PHB may be not important in nitrogen-fixing nodules and the role of PHB during symbiosis could be a store of excess reductant rather than a carbon buffer (20). However, 3-hydroxybutyrate dehydrogenase (BdhA) acting downstream of PhaZ in the PHB degradation pathway is required for effective symbiosis of NGR234 on *L. leucocephala* but not *Tephrosia vogelii*, *Macroptilium atropurpureum*, or *V. unguiculata* plants (42). These findings suggest that the importance of PHB degradation can vary in different symbiosis systems and a buildup of 3-hydroxybutyrate could inhibit the symbiosis in certain cases.

It should be noted that the Δ*phbC1C2* mutant of NGR234 still formed pink nodules and leaf chlorophyll content of inoculated *V. unguiculata* plants was similar to those inoculated with the wild-type NGR234. This is in line with results indicating that the *phbC* mutant of *S. meliloti* Rm1021 was able to fix nitrogen, though a host-dependent (*Medi truncatula* versus *M. sativa*) variation of nitrogenase activity was observed (23). However, host plants inoculated with these *phbC* mutants of *Sinorhizobium* exhibited a significant reduction in shoot dry weight and nodule occupancy as described above. The *phbC* mutant of *A. caulinodans* was Fix^- in symbiosis with *Sesbania rostrata* (29), while an *R. etli* mutant lacking a functional PHB synthase exhibited a prolonged capacity to fix nitrogen in nodules of *Phaseolus vulgaris* (28). Therefore, PHB synthase can be involved in optimizing symbiosis in a rhizobium-host-dependent manner, or even in a way interacting with changing environments, as implied in a study of *Rhizobium leguminosarum* strains nodulating pea and bean (43).

Distinct roles of different phasins in regulating number and size of PHB granules. Although PHB is thought as a source of carbon and energy for different cellular processes during adaptation and survival in the environment, a recent advance in this field has highlighted an active role of multifaceted phasins in reducing the deleterious effects of diverse stresses (13). Constitutively expressed fusion with eYFP has been developed as an effective tool to determine whether candidate proteins represent true GAPs of PHB (18, 44). In this study, four PhaPs harboring the Phasin_2 domain were demonstrated to colocalize with PHB granules under free-living condition using the same technique. In *S. meliloti* Rm1021, two putative phasins named as PhaP1 and PhaP2, showing 88.4% and 89.3% identity to PhaP1 and PhaP2 of NGR234, respectively, were redundant regarding their role in PHB production and symbiotic performance (27). However, four PhaPs in NGR234 seem to be differentially involved in PHB production under either free-living or symbiotic conditions.

At stationary phase, PhaP2 was the most abundant phasin on PHB granules of NGR234. Indeed, the Δ*phaP2* mutant showed the most drastic change in PHB granule size among individual mutants of phasin genes. This is similar to the finding in *R. eutropha* H16 and *B. diazoefficiens* USDA110, in which $PhaP1_{Reu}$ and $PhaP4_{Bdi}$, respectively, were the major phasin proteins (1, 30, 45). In contrast, PhaP1 and PhaP2 in *S. meliloti* Rm1021 made roughly equal contributions, as no obvious difference in either the size or number of PHB granules was found between individual *phaP1* and *phaP2* mutants (27). The *phaP1P2* double mutant of Rm1021 had no detectable PHB granules (27), and this is in line with a significantly reduced number of PHB granules in the Δ*phaP1P2* mutant compared to mutants lacking individual phasins and the other double mutants of NGR234 at stationary phase. Moreover, among diverse putative GAPs, PhaP1 was the most abundant one on PHB granules in the Δ*phaP2* mutant of NGR234. These findings indicate that PhaP1 together with the major phasin PhaP2 is crucial for regulating PHB granule number in free-living cultures of NGR234. Although *phaP3* and *phaP4* had relatively low transcript levels under free-living conditions (32), a reduced number of PHB granules could also be observed in individual *phaP3* and *phaP4* mutants at stationary phase, indicating cumulative contributions by PhaP3 and PhaP4. The relatively lower importance of minority phasins was also reported for *R.*

eutropha (18, 46), though $PhaP5_{Reu}$, $PhaP6_{Reu}$, and $PhaP7_{Reu}$ had distinct subcellular localizations (18).

Differential transcriptional profiles of different phasins have been reported for *B. diazoefficiens* USDA110 grown in different media (30). In *R. eutropha* H16, $PhaP6_{Reu}$ and $PhaP7_{Reu}$ could associate with PHB granules later than the other phasins (18). In contrast to the other three phasins, PhaP3 was not detected on PHB granules collected from free-living NGR234, possibly due to its lowest transcription level among these phasin genes in cultures (32). Instead, *phaP3* located on the symbiosis plasmid was upregulated within *V. unguiculata* nodules (32). In line with these findings, the numbers of PHB granules in the Δ*phaP1P3*, Δ*phaP2P3*, and Δ*phaP1P2P3* mutants compared to the Δ*phaP1*, Δ*phaP2*, and Δ*phaP1P2* mutants, respectively, were similar at stationary phase but significantly lower within *V. unguiculata* nodules. Therefore, PhaP3 may play a more active role in regulating PHB granule number during symbiosis than in free-living cultures. The *phaP4* gene was also upregulated in *V. unguiculata* nodules (to a lesser extent than *phaP3*) (32) and made a cumulative contribution to PHB biosynthesis.

It was reported that the *phaP1P2* mutant of *S. meliloti* Rm1021 lacking PHB granules was able to fix nitrogen but that the shoot dry weight of inoculated *M. truncatula* plants was reduced compared to that of the wild-type strain (27). This Fix^+ Eff^- phenotype has also been reported for a *glnD* mutant of Rm1021 (47) and *hemN1* mutants of *S. fredii* CCBAU45436 and *Sinorhizobium* sp. CCBAU05631 nodulating wild soybean (48). In this study, *V. unguiculata* plants inoculated with the Δ*phaP1P2* or Δ*phaP2P3* mutant of NGR234 exhibited slight but nonsignificant reduction in shoot dry weight compared to that of plants inoculated with the wild-type strain. Bacteroids of these two double mutants, as well as Δ*phaP1P2P3* and Δ*phaP1P2P3P4* bacteroids, had a reduced number of PHB granules, whereas no granules were observed in free-living cells of the Δ*phaP1P2P3* or Δ*phaP1P2P3P4* mutant.

Additional functions of phasins have been proposed, such as protective effect and chaperone activity (13). It was reported that a phasin from *Azotobacter* sp. FA8 can enhance the resistance of non-PHB-producing *E. coli* to both heat shock and superoxide stress, possibly by exerting chaperone-like activity (11). In the analysis of GAPs, PHB granules of the Δ*phaP1P2* mutant at stationary phase had a lower abundance of phasin than the Δ*phaP1* and Δ*phaP2* mutants, while some other proteins of diverse functions were identified as putative GAPs, such as a small heat shock protein (NGR_c28710), oxidoreductase (NGR_c21410), sarcosine oxidase (NGR_c29020), and uridylyltransferase (NGR_b18390). This suggests that phasins may prevent PHB granules from associating with proteins of other cellular pathways by occupying the granule surface. For example, the most abundant GAPs identified in this study are those of unknown function and those involved in energy production/conversion and signal transduction. Although we could not exclude the probability of false-positive GAPs during the sample preparation, identification of GAPs of low abundance, multiple subcellular localizations, and those bound loosely to PHB granules is also possible, as discussed in a previous study of GAPs of PHB in *R. eutropha* H16 (49). For example, NGR_b13620, NGR_c33730, and NGR_b19160, of low abundance identified by the nanospray ESI-MS analysis in this study, were demonstrated as true GAPs in the subcellular colocalization experiments.

The low similarity levels among four PhaPs in NGR234 and their distinct transcription patterns under free-living and symbiotic conditions could lead to a complex interaction network, which remains unexplored. This hypothesis is supported by the distinct metabolic profiles of single or multiple mutants of PhaPs. It is noteworthy that in contrast to the conserved PhaP1 and PhaP2, accessory PhaP3 and PhaP4 have a restricted phyletic distribution in *Sinorhizobium*. This further supports the view that accessory functions have been extensively integrated into the core regulation network during environmental adaptation of rhizobia (34, 50–52).

Conclusions. Among diverse GAPs of PHB, PhaP1, PhaP2, PhaP3, and PhaP4 were demonstrated as true phasins with distinct phyletic distribution patterns and transcriptional profiles. The conserved PhaP2 is the dominant phasin regulating PHB granule size

under both free-living and symbiotic conditions. In free-living cells at stationary phase, the conserved PhaP1 and accessory PhaP3 and PhaP4 also contribute to the regulation of PHB granule number and size. The accessory *phaP3* gene, located on the symbiosis plasmid and upregulated in nodules, and *phaP2* are crucial in regulating PHB biosynthesis in nodules, and PhaP4 and PhaP1 made cumulative contributions. Under the test conditions, this study revealed the essential role of PHB synthases rather than PHB depolymerase or phasins of NGR234 in symbiotic interaction with *V. unguiculata*. The presence or absence of PHB granules could not account for the contrasting phenotypes of test mutants. Metabolic profiles of these mutants were strain specific under free-living conditions and should be further investigated in nodules. Variations in the pool of GAPs in representative *phaP* mutants imply that PHB is not just a store of carbon and reductant but may actively interact with other cellular pathways through direct binding of related proteins, particularly when the diversity and abundance of different phasins, the major components of the PHB granule cover, change under the fluctuating environmental conditions. These findings are also significant in the context of evolution, as core and accessory PhaPs play coordinated roles in these processes, highlighting the importance of integration between accessory and core functions during bacterial adaptations.

MATERIALS AND METHODS

Bacterial strains and growth conditions. Bacterial strains and plasmids used in this study are shown in Table 1. *E. coli* was grown at 37°C in Luria broth (LB) medium supplemented with appropriate antibiotics. The broad-host-range strain *S. fredii* NGR234 (53) was grown at 28°C in TY medium (tryptone at 5 g/liter, yeast extract at 3 g/liter, and $CaCl_2$ at 0.6 g/liter). *S. fredii* NGR234 is resistant to rifampin (Rif). The antibiotic concentrations used were 50 μg/ml of Rif, 50 μg/ml of kanamycin (Km), 30 μg/ml of gentamicin (Gen), and 10 μg/ml of tetracycline (Tet). The sucrose concentration for screening double-crossover mutant strains was 5% (wt/vol).

Construction of mutants and complemented strains. The primers used in this study are listed in Table 2. For precise deletion of coding sequences of *phbC1*, *phbC2*, *phaP1*, *phaP2*, *phaP3*, and *phaP4* (*NGR_b11320*), a seamless assembly cloning kit (Taihe Biotechnology, Beijing, China) was used to construct knockout vectors derived from pJQ200SK (54). Briefly, 500- to 700-bp upstream and downstream fragments of target gene were amplified using primers (Table 2) carrying sequences corresponding to the ends of SmaI restriction sites in pJQ200SK. These two fragments were simultaneously mixed with linearized pJQ200SK (digested by SmaI) and incubated at 50°C for 15 min, and the positive *E. coli* clones were selected by antibiotic resistance and colony PCR after transformation. Then the integrative plasmid was conjugated into the wild-type NGR234 by triparental mating using the helper plasmid pRK2013 (55). Single-crossover clones were screened using a TY (Rif Gen) plate and by colony PCR. The resultant clones were cultured in liquid TY medium (Rif) for 24 to 36 h and screened on a TY (Rif) plate containing 5% sucrose. Double-crossover clones were verified by colony PCR and Sanger sequencing. The same method was used to construct double and multiple mutants. To generate the *phaZ* (*NGR_b03370*) mutant, an intragenic fragment of 388 bp, amplified using primers *phaZ*F_BamHI and *phaZ*R_XbaI, was digested by BamHI and XbaI and linked with the pVO155 (56) digested with the same endonucleases. The resultant vector was conjugated into NGR234. The *NGR_b03370* mutant was selected on a TY (Rif Km) plate, followed by PCR verification. For the construction of the *phbC1C2* double mutant, which served as a control in subcellular localization of PhaP1, PhaP2, and PhaP3, the *cre-lox* system was used (57). First, a 530-bp DNA fragment upstream and a 683-bp DNA fragment downstream from the coding sequence of *phbC1* were amplified and ligated to pCM351 suicide plasmid using corresponding primers and endonucleases listed in Table 2. The resultant plasmid was conjugated into NGR234 through triparental mating with pRK2013 as the helper plasmid. The *phbC1* mutant sensitive to Tet and resistant to Gen was selected. Then a pVO155 derivative carrying a 397-bp intragenic fragment of the *phbC2* gene was constructed and conjugated into the *phbC1* mutant using the same procedure as described above for the construction of the *NGR_b03370* mutant. All constructed mutants were verified using PCR and Sanger sequencing. To perform a genetic complementation, the integrative pJQ200SK plasmid carrying corresponding gene (*phaP3* or *phbC2*), upstream and downstream fragments of the gene was conjugated into mutant by triparental mating with pRK2013 helper plasmid. Primers used in this study are listed in Table 2. Single-crossover and subsequent double-crossover clones were screened and verified using the same method as the mutant construction using pJQ200SK plasmid. This allowed a complementation event with the cloned DNA being inserted into its original genome location by double crossover.

Construction of strains carrying fusion proteins with eYFP. The empty fusion vector pBBR1MCS-2-P_{phaC}-*eyfp*-n1 carries the *eyfp* (enhanced yellow fluorescent protein) gene under the control of the constitutive *phaCAB* promoter of *R. eutropha* (44). Test genes (*phaP1*, *phaP2*, *phaP3*, *NGR_b11320*, *NGR_b13620*, *NGR_c33730*, and *NGR_b19160*) were amplified using primers listed in Table 2 and cloned in frame to the N terminus of the *eyfp* gene using corresponding endonucleases. The *target_gene-eyfp* fusion vector was conjugated into NGR234 by triparental mating using pRK2013 as the helper plasmid. The antibiotic resistance marker of pBBR1MCS-2-P_{phaC}-*eyfp*-n1 (Km^r) is the same as that of the *phbC1C2*

TABLE 1 Plasmid and strains used in this study

Plasmid or strain	Characteristics[a]	Reference
Plasmids		
pCM351	Gen^r Tet^r; broad-host-range *cre-lox* vector	57
pJQ200SK	Gen^r; P15A origin from pACYC184; *lacZ sacB traJ*	54
pVO155	Km^r; pUC119 derivative for insertion into genome	56
pBBR1MCS-2	Km^r; broad-host-range vector	58
pBBR1MCS-3	Tet^r; broad-host-range vector	58
pRK2013	Km^r; ColE1 replicon, *tra*$^+$ from RK2	55
pBBR1MCS-2-P$_{phaC}$-*eyfp*-n1	Km^r; universal vector for construction of fusions N terminal to *eyfp* under the control of the *phaCAB* promoter	44
pBBR1MCS-3-P$_{phaC}$-*eyfp*-n1	Tet^r; universal vector for construction of fusions N terminal to *eyfp* under the control of the *phaCAB* promoter	This work
pBBR1MCS-2-P$_{phaC}$-*phaP1-eyfp*	Km^r; N-terminal fusion of PhaP1 to eYFP	This work
pBBR1MCS-2-P$_{phaC}$-*phaP2-eyfp*	Km^r; N-terminal fusion of PhaP2 to eYFP	This work
pBBR1MCS-2-P$_{phaC}$-*phaP3-eyfp*	Km^r; N-terminal fusion of PhaP3 to eYFP	This work
pBBR1MCS-3-P$_{phaC}$-*phaP1-eyfp*	Tet^r; N-terminal fusion of PhaP1 to eYFP	This work
pBBR1MCS-3-P$_{phaC}$-*phaP2-eyfp*	Tet^r; N-terminal fusion of PhaP2 to eYFP	This work
pBBR1MCS-3-P$_{phaC}$-*phaP3-eyfp*	Tet^r; N-terminal fusion of PhaP3 to eYFP	This work
pBBR1MCS-2-P$_{phaC}$-b11320-*eyfp*	Km^r; N-terminal fusion of NGR_b11320 to eYFP	This work
pBBR1MCS-2-P$_{phaC}$-b13620-*eyfp*	Km^r; N-terminal fusion of NGR_b13620 to eYFP	This work
pBBR1MCS-2-P$_{phaC}$-c33730-*eyfp*	Km^r; N-terminal fusion of NGR_c33730 to eYFP	This work
pBBR1MCS-2-P$_{phaC}$-b19160-*eyfp*	Km^r; N-terminal fusion of NGR_b19160 to eYFP	This work
pJQ200SK-*phbC2*	Gen^r; pJQ200SK carrying *phbC2* for *in situ* complementation	This work
pJQ200SK-*phaP3*	Gen^r; pJQ200SK carrying *phaP3* for *in situ* complementation	This work
Strains		
Escherichia coli DH5α	F$^-$ φ80*lacZ*ΔM15 Δ(*lacZYA-argF*) *U169 deoR recA1 endA1 hsdR17*(r_k^- m_k^+) *phoA supE44* λ^- *thi-1 gyrA96 relA1*	
Sinorhizobium fredii		
NGR234	Rif^r; wild type	53
phbC1 strain	Rif^r Gen^r; NGR234 Δ*phbC1*::Gen	This work
phbC1C2 strain	Rif^r Gen^r Km^r; NGR234 Δ*phbC1*::Gen with pVO155 inserted into *phbC2*	This work
Δ*phbC1* strain	Rif^r; NGR234 with *phbC1* precise deletion	This work
Δ*phbC2* strain	Rif^r; NGR234 with *phbC2* precise deletion	This work
Δ*phbC1C2* strain	Rif^r; NGR234 with *phbC1* and *phbC2* precise deletion	This work
Δ*phbC1C2*+*C2* strain	Rif^r; Δ*phbC1C2* strain complemented with *phbC2*	This work
phaZ (*NGR_b03370*) strain	Rif^r Km^r; NGR234 with pVO155 inserted into *NGR_b03370*	This work
Δ*phaP1* strain	Rif^r; NGR234 with *phaP1* precise deletion	This work
Δ*phaP2* strain	Rif^r; NGR234 with *phaP2* precise deletion	This work
Δ*phaP3* strain	Rif^r; NGR234 with *phaP3* precise deletion	This work
Δ*phaP4* strain	Rif^r; NGR234 with *phaP4* precise deletion	This work
Δ*phaP1P2* strain	Rif^r; NGR234 with *phaP1* and *phaP2* precise deletions	This work
Δ*phaP1P3* strain	Rif^r; NGR234 with *phaP1* and *phaP3* precise deletions	This work
Δ*phaP2P3* strain	Rif^r; NGR234 with *phaP2* and *phaP3* precise deletions	This work
Δ*phaP2P3*+*P3* strain	Rif^r; Δ*phaP2P3* strain complemented with *phaP3*	This work
Δ*phaP1P2P3* strain	Rif^r; NGR234 with *phaP1*, *phaP2*, and *phaP3* precise deletions	This work
Δ*phaP1P2P3P4* strain	Rif^r; NGR234 with *phaP1*, *phaP2*, *phaP3*, and *phaP4* precise deletions	This work

[a]Gen^r, gentamicin resistance; Tet^r, tetracycline resistance; Km^r, kanamycin resistance; Rif^r, rifampin resistance.

mutant (Rif^r Km^r). The P$_{phaC}$-*target_gene-eyfp* fragment carrying *phaP1*, *phaP2*, or *phaP3* was further amplified using primers P123F_KpnI and P123R_SpeI and cloned into pBBR1MCS-3 (58) using the seamless assembly cloning kit. The resultant pBBR1MCS-3-derived fusion vectors for *phaP1*, *phaP2*, and *phaP3* were individually conjugated into the *phbC1C2* mutant (Rif^r Km^r). To simplify further experiments, a marker-free deletion mutant, the Δ*phbC1C2* mutant, was constructed as described above using pJQ200SK. The pBBR1MCS-2-P$_{phaC}$-*eyfp*-n1-derived fusion vectors for *phaP4* (*NGR_b11320*), *NGR_b13620*, *NGR_c33730*, and *NGR_b19160* were conjugated into this Δ*phbC1C2* mutant as controls for subcellular colocalization experiments. All constructed vectors and strains carrying them were verified by PCR and Sanger sequencing.

Plant assay. Seeds of *V. unguiculata* were surface sterilized in 17% (vol/vol) sodium hypochlorite solution for 5 min and washed five times using autoclaved deionized water. Then the treated seeds were germinated on 0.5% agar plates at 28°C in the dark for 48 h. Seedlings were inoculated with 1 ml of suspension (OD_{600} = 0.2) of rhizobia in 0.8% (wt/vol) NaCl solution and grown in vermiculite moistened with low-N nutrient solution [$Ca(NO_3)_2{\cdot}4H_2O$ at 0.03 g, KCl at 0.075 g, $MgSO_4$ at 0.06 g, K_2HPO_4 at 0.136 g, $CaSO_4{\cdot}2H_2O$ at 0.46 g, $FeC_6H_5O_7$ at 0.075 g, H_3BO_3 at 2.86 mg, $MnSO_4$ at 1.81 mg, $CuSO_4{\cdot}5H_2O$ at 0.8 mg, $ZnSO_4$ at 0.22 mg, and H_2MoO_4 at 0.02 mg per liter of distilled water] in Leonard jars (59) at 25°C with a 12-h illumination period and harvested 30 days postinoculation (dpi). Leaf relative chlorophyll concentration was detected by a SPAD-502 meter (Konica Minolta) as described previously (22, 60). To

TABLE 2 Primers used in this study

Primer	DNA sequence (5′–3′)[a]	Description
*phaP1*F_NdeI	GGGAATTC**CATATG**GCTACCAAGAAGACCGAA	For construction of *phaP1-eyfp* fusion
*phaP1*R_BamHI	CG**GGATCC**CCGGCCTTCTTGAAGGTGGAG	
*phaP2*F_NdeI	GGGAATTC**CATATG**TTTAATTTCGACGACGCAAA	For construction of *phaP2-eyfp* fusion
*phaP2*R_BamHI	CG**GGATCC**CCGGCGGCGGCAGCAGACTTCA	
*phaP3*F_NdeI	GGGAATTC**CATATG**TCCAGGACCGCAGAAAAGC	For construction of *phaP3-eyfp* fusion
*phaP3*R_XmaI	CG**CCCGGG**CGGCCGTCTTGAGGTCTGCTA	
P123F_KpnI	*CTAAAGGGAACAAAAGCTG***GGTACC**CAAAAATTCATCCTTCTCG	To transfer *phaP1-*, *phaP2-*, or *phaP3-eyfp* fusion into pBBR1MCS-3
P123R_SpeI	*CGGTGGCGGCCGCTCTAGA***ACTAGT**TTACTTGTACAGCTCGTCC	
MCS-3F_SpeI	**ACTAGT**TCTAGAGCGGCCG	For generation of linear pBBR1MCS-3 plasmid
MCS-3R_KpnI	**GGTACC**CAGCTTTTGTTCC	
*NGR_b11320*F	*AGTCGACGGTACCGCGGGCC*ATGTCGAAGAAAATATCCGAC	For construction of *NGR_b11320-eyfp* fusion
*NGR_b11320*R	*GGTGGCGACCGGTGGATCCC*GCATGACCATCTGCCGC	
*NGR_b13620*F	*AGTCGACGGTACCGCGGGCC*ATGCCCAAGCAATCCACC	For construction of *NGR_b13620-eyfp* fusion
*NGR_b13620*R	*GGTGGCGACCGGTGGATCCC*GGGATGTCCTGCGCTCGC	
*NGR_c33730*F	*AGTCGACGGTACCGCGGGCC*ATGTTCTACCAGCTTTACGAA	For construction of *NGR_c33730-eyfp* fusion
*NGR_c33730*R	*GGTGGCGACCGGTGGATCCC*GGGCCGATTTGCCGC	
*NGR_b19160*F	*AGTCGACGGTACCGCGGGCC*ATGGCGAAAGTAATCGTTGT	For construction of *NGR_b19160-eyfp* fusion
*NGR_b19160*R	*GGTGGCGACCGGTGGATCCC*GTGCTGCCCTCCGTCC	
*phbC1*upF_EcoRI	G**GAATTC**ACTGCTGCGCTACAAT	For *phbC1* deletion
*phbC1*upR_NdeI	GGAATTC**CATATG**GTCGATCACCCGTCTT	
*phbC1*downF_AgeI	G**ACCGGT**AAAGAGGCTATCCCCC	For *phbC1* deletion
*phbC1*downR_SacI	GGC**GAGCTC**CGCAAACAGAAACAAA	
*phbC2*F_BamHI	CG**GGATCC**AGCAAGTTTGCCATCG	For *phbC2* insertion
*phbC2*R_XbaI	GC**TCTAGA**CATGGAGCGCCAGCGT	
*phaZ*F_BamHI	CG**GGATCC**GCTGCGCGACAATAAC	For *phaZ* insertion
*phaZ*R_XbaI	GC**TCTAGA**ATCGTTCGTCCCGTGC	
*phbC1*upF	ATATCGAATTCCTGCAGCCCACTGCTGCGCTACAAT	For *phbC1* precise deletion by pJQ200SK
*phbC1*upR	TAGCCTCTTTGTCGATCACCCGTCTT	
*phbC1*downF	GGTGATCGACAAAGAGGCTATCCCCC	For *phbC1* precise deletion by pJQ200SK
*phbC1*downR	CTAGAACTAGTGGATCCCCCTCGCACGATACGAGAC	
*phbC2*upF	ATATCGAATTCCTGCAGCCCTTCGGCAATCGCTCAA	For *phbC2* precise deletion and *in situ* complementation by pJQ200SK
*phbC2*upR	TTTGCCTTCTGTTCGACCGATTTGGG	For *phbC2* precise deletion by pJQ200SK
*phbC2*downF	TCGGTCGAACAGAAGGCAAAGGAGAC	For *phbC2* precise deletion by pJQ200SK
*phbC2*downR	CTAGAACTAGTGGATCCCCCAAATGGACGTTCTTCA	For *phbC2* precise deletion and *in situ* complementation by pJQ200SK
*phaP1*upF	ATATCGAATTCCTGCAGCCCCAACTGGCGCAGGGAGA	For *phaP1* precise deletion by pJQ200SK
*phaP1*upR	CGGCGGCTTCGGCCGGGTCAAAGGAAA	
*phaP1*downF	TGACCCGGCCGAAGCCGCCGAAAAGG	For *phaP1* precise deletion by pJQ200SK
*phaP1*downR	CTAGAACTAGTGGATCCCCCCTGCACAACTACATCGCCC	
*phaP2*upF	ATATCGAATTCCTGCAGCCCGCGATAATCCAATGCGTTAC	For *phaP2* precise deletion by pJQ200SK
*phaP2*upR	TCAGGCGGCGTGCTTTTCTTGTTTGCGTC	
*phaP2*downF	AAGAAAAGCACGCCGCCTGACGATAT	For *phaP2* precise deletion by pJQ200SK
*phaP2*downR	CTAGAACTAGTGGATCCCCCGCCGCATTCTCCAACG	
*phaP3*upF	ATATCGAATTCCTGCAGCCCAACTTGATAGTCGCTTCGT	For *phaP3* precise deletion and *in situ* complementation by pJQ200SK
*phaP3*upR	ACGGCAATCACGAAGCCAATCAAGGAAT	For *phaP3* precise deletion by pJQ200SK
*phaP3*downF	ATTGGCTTCGTGATTGCCGTGGATTGAC	For *phaP3* precise deletion by pJQ200SK
*phaP3*downR	CTAGAACTAGTGGATCCCCCTGATGGTAGTGCAGGCGA	For *phaP3* precise deletion and *in situ* complementation by pJQ200SK
*phaP4*upF	CTTGATATCGAATTCCTGCAGCCCCCAGCTTGCCCAGACGA	For *phaP4* precise deletion by pJQ200SK
*phaP4*upR	TGCACCCGCAACCAGCGAAGAACAGGAGGAAC	
*phaP4*downF	TGTTCTTCGCTGGTTGCGGGTGCAAGTG	For *phaP4* precise deletion by pJQ200SK
*phaP4*downR	CGCTCTAGAACTAGTGGATCCCCCGCACGCTCTTCCACTGTT	

[a]Restriction sites are in bold, the sequences at the ends of SmaI restriction sites in pJQ200SK are underlined, and the sequences at the end of the linear plasmid pBBR1MCS-2 or pBBR1MCS-3 are in italics.

minimize the sampling error, three leaflets of the third leaf were tested for each plant. The shoot dry weight was tested after drying in an oven at 60°C for 5 days. Nodules were used for preparing samples for transmission electron microscopy (TEM). For competitive nodulation, seedlings were inoculated with 1 ml of an inoculum combining equal volumes of bacterial suspension ($OD_{600} = 0.2$) of the wild type and mutant strains. Nodules of five plants for each treatment were collected 30 dpi and surface sterilized in 17% (vol/vol) sodium hypochlorite solution for 5 min. After washing five times with autoclaved deionized water, the nodules were crushed. Bacteria from each nodule were cultured on a TY plate continuously at 28°C for 3 days. Colony PCR was used to identify the wild type and mutants. At least two independent experiments were carried out.

TEM. Bacterial cultures (1 ml) were harvested at stationary phase by centrifugation for 5 min at 8,000 × *g*. The pellets or nodules were fixed in 2.5% glutaraldehyde in 0.05 M cacodylate buffer (61). The resultant samples were washed with 0.1 M phosphate buffer and postfixed in the same buffer containing 1% (wt/vol) OsO_4. The samples were washed again with 0.1 M phosphate buffer and dehydrated with increasing volumes of acetone (30%, 50%, 70%, 90%, and 100%). The samples embedded in Spurr epoxy were then cut into ultrathin sections (80 nm thick) using a Leica Ultracut C6i. The sections were stained with uranyl acetate and lead citrate and observed with a JEM-1230 transmission electron microscope. To determine the size and number of PHB granules by ImageJ software, 30 pictures (magnification, 25,000×) for cells from one free-living culture of each test strain and 15 pictures (mutants or complemented strains; magnification, 20,000×) or 10 pictures (wild-type NGR234; magnification, 20,000×) of 3 or 4 nodules from different plants were taken by the microscope. For each picture, five bacterial cells located on the diagonal line were selected for the determination of size and number of PHB granules.

Laser scanning confocal microscopy. Stationary-phase cultures of strains carrying the eYFP-tagged fusions were collected and suspended in 0.8% sodium chloride and stained by addition of 0.01 volume of Nile red solution (100 μg of Nile red/ml of dimethyl sulfoxide) in the dark for 5 min. Nile red fluorescent dye was used for staining cellular PHB granules (62). The stained cells were washed once with 0.8% sodium chloride. Isometric stained cell culture and 1% agarose solution were mixed together to fix the cells, which were subsequently observed with an Olympus laser scanning confocal microscope using Olympus Fluoview version 4.0b software. The excitation light source was set to 488 nm (green fluorescent protein [GFP] channel) for detection of the eYFP signal and 546 nm (RFP-Channel) for Nile red signal.

Biolog metabolic assay. A Biolog GEN III microplate (71 carbon source utilization assays and 23 chemical sensitivity assays) was used to compare metabolic profiles of test strains. The colonies of test strains on TY plates were individually suspended in the inoculating fluid IF-A (Biolog GEN III identification fluids, catalog no. 72401), and 100 μl of bacterial suspension was added into each well of the microplate. Then the microplates were incubated at 28°C for 72 h. Absorbance reading at 590 nm was carried out every 12 h using Biolog MicroStation system, and active (2), weak (1), or no (0) growth in each well was automatically defined by the integrated software of Biolog. Three independent experiments were performed for each strain.

Isolation and purification of PHB granules. PHB granules were isolated by a method of two steps of sucrose density gradient centrifugation, modified from that described earlier (63). Briefly, 300-ml quantities of bacterial cultures grown in liquid TY medium were collected at stationary phase by centrifugation (5 min, 8000 × *g*, and 4°C) and washed once with 10 ml of potassium phosphate buffer (100 mM, pH 7.5). The pellets were ground into powder in the presence of liquid nitrogen. The bacterial powder was suspended and sonicated in 10 ml of Tris-HCl (10 mM, pH 8.0). After centrifugation, the insoluble fraction containing PHB granules was suspended with 5 ml Tris-HCl (10 mM, pH 8.0) and subject to ultracentrifugation (15 h, 28,000 × *g*, and 4°C, with a Beckman SW28 rotor) in a sucrose gradient. The gradient was prepared from 18 ml of 1.66 M, 8 ml of 1.33 M, and 8 ml of 1 M sucrose in Tris-HCl (10 mM, pH 8.0). The PHB granule layer (located between 1.66 M and 1.33 M sucrose solution) was separated and washed once with Tris-HCl (10 mM, pH 8.0). To improve the quality of purification, a second-round centrifugation in a sucrose gradient (15 h, 28,000 × *g*, and 4°C, with a Beckman SW28 rotor) was carried out. The gradient was prepared from 8 ml of 2 M, 14 ml of 1.66 M, 8 ml of 1.33 M, and 8 ml of 1 M sucrose in Tris-HCl (10 mM, pH 8.0). After ultracentrifugation, the PHB granules were washed twice with Tris-HCl (10 mM, pH 8.0) and then stored at −20°C.

SDS-PAGE To obtain a global view of granule-associated proteins (GAPs) of PHB, granule pellets from representative strains were suspended with 1× loading buffer (0.6% [wt/vol] SDS, 1.25% [wt/vol] β-mercaptoethanol, 0.25 mM EDTA, 10% [vol/vol] glycerol, 0.001% [wt/vol] bromophenol blue, 12.5 mM Tris-HCl [pH 6.8]) and boiled at 100°C for 5 min. Then 20-μg quantities of proteins were separated by SDS-PAGE (polyacrylamide gel electrophoresis; 5% stacking gel, 15% separating gel, 0.1% SDS) and stained with Coomassie brilliant blue R-250.

Mass spectrometry analysis. PHB granules were resuspended in a urea-sulfocarbamide solution (3.04 g of urea and 8.4 g of sulfocarbamide in 20 ml of double-distilled water [ddH_2O]), in which GAPs from the surface of PHB granules were dissolved. After centrifugation (20 min and 14,000 × *g*), the supernatants were quantified by the Bradford method. Then 50 μg of GAPs from each strain was digested to peptide by trypsin. Nano-liquid chromatography (nano-LC) separation was achieved with a Waters (Milford, MA) nanoACQUITY nano-high-performance liquid chromatograph (nano-HPLC). Nanospray ESI-MS was performed on a Thermo Q-Exactive high-resolution mass spectrometer (Thermo Scientific, Waltham, MA) with a 70,000 MS scan resolution, 17,500 tandem MS (MS/MS) scan resolution, and top-10 MS/MS selection. Raw data from the mass spectrometer were preprocessed with Mascot Distiller 2.4 (Matrix Science, London, UK) for peak picking. The resultant peak lists were searched against an *S. fredii* NGR234 protein database using the Mascot 2.5 search engine (Matrix Science). The search parameters were as follows: carbamidomethyl as fixed modification of cysteine, oxidation of methionine and phosphorylation of serine, threonine, and tyrosine as variable modifications, two maximum missed cleavages for trypsin, MS mass tolerance of 10 ppm, and MS/MS mass tolerance of 0.02 Da. The exponentially modified protein abundance index (emPAI = 10^{PAI} − 1, where PAI is the ratio of observed number of peptides per protein and observable number of peptides per protein), a label-free quantitative measure of protein abundance in proteomics (64), was used to determine the abundances of different GAPs.

Quantification of PHB. Bacterial cultures (40 ml) in TY medium were collected at stationary phase by centrifugation (4 min and 13,000 × *g*). Then the cell pellets were homogenized with sodium hypochlorite at 37°C for 1 h. After centrifugation (20 min and 13,000 × *g*), the pellets were washed with 2 ml

of ddH_2O and precipitated with 2 ml of 1:1 alcohol-acetone. The pellets were resuspended in 2 ml of chloroform, and 100 μl of solution was used for determination of PHB levels after centrifugation (20 min and 14,000 $\times$ *g*). PHB was determined as chrotonic acid in 10 ml of H_2SO_4 (65, 66). For PHB quantification of bacteroids, 130- to 160-mg nodules (10 to 15 nodules randomly selected from five plants) were crushed with liquid nitrogen before homogenization with sodium hypochlorite at 37°C for 1 h. Three subsamples of stationary-phase cultures or nodules were used in PHB determination. Three independent experiments were performed.

SUPPLEMENTAL MATERIAL

Supplemental material for this article may be found at https://doi.org/10.1128/AEM.00717-19.

SUPPLEMENTAL FILE 1, PDF file, 6.2 MB.

SUPPLEMENTAL FILE 2, XLSX file, 0.03 MB.

SUPPLEMENTAL FILE 3, XLSX file, 1.1 MB.

ACKNOWLEDGMENTS

We thank Dieter Jendrossek from Universität Stuttgart for providing the vector carrying eYFP.

This work was supported by the National Natural Science Foundation of China (31522003), the National Basic Research Program of China (973 program 2015CB158301), and the Innovative Project of State Key Laboratory of Agrobiotechnology (2018SKLAB1-2).

We declare that we do not have any commercial or associative interest connected with the work described here.

REFERENCES

1. Maestro B, Sanz JM. 2017. Polyhydroxyalkanoate-associated phasins as phylogenetically heterogeneous, multipurpose proteins. Microb Biotechnol 10:1323–1337. https://doi.org/10.1111/1751-7915.12718.
2. Jendrossek D, Pfeiffer D. 2014. New insights in the formation of polyhydroxyalkanoate granules (carbonosomes) and novel functions of poly (3-hydroxybutyrate). Environ Microbiol 16:2357–2373. https://doi.org/10.1111/1462-2920.12356.
3. Kadouri D, Jurkevitch E, Okon Y. 2003. Involvement of the reserve material poly-β-hydroxybutyrate in *Azospirillum brasilense* stress endurance and root colonization. Appl Environ Microbiol 69:3244–3250. https://doi.org/10.1128/aem.69.6.3244-3250.2003.
4. Wang Q, Yu H, Xia Y, Kang Z, Qi Q. 2009. Complete PHB mobilization in *Escherichia coli* enhances the stress tolerance: a potential biotechnological application. Microb Cell Fact 8:47. https://doi.org/10.1186/1475-2859-8-47.
5. Zhao YH, Li HM, Qin LF, Wang HH, Chen GQ. 2007. Disruption of the polyhydroxyalkanoate synthase gene in *Aeromonas hydrophila* reduces its survival ability under stress conditions. FEMS Microbiol Lett 276:34–41. https://doi.org/10.1111/j.1574-6968.2007.00904.x.
6. Koskimäki JJ, Kajula M, Hokkanen J, Ihantola EL, Kim JH, Hautajärvi H, Hankala E, Suokas M, Pohjanen J, Podolich O, Kozyrovska N, Turpeinen A, Pääkkönen M, Mattila S, Campbell BC, Pirttilä AM. 2016. Methyl-esterified 3-hydroxybutyrate oligomers protect bacteria from hydroxyl radicals. Nat Chem Biol 12:332–338. https://doi.org/10.1038/nchembio.2043.
7. Nowroth V, Marquart L, Jendrossek D. 2016. Low temperature-induced viable but not culturable state of *Ralstonia eutropha* and its relationship to accumulated polyhydroxybutyrate. FEMS Microbiol Lett 363:fnw249. https://doi.org/10.1093/femsle/fnw249.
8. Obruca S, Sedlacek P, Koller M, Kucera D, Pernicova I. 2018. Involvement of polyhydroxyalkanoates in stress resistance of microbial cells: biotechnological consequences and applications. Biotechnol Adv 36:856–870. https://doi.org/10.1016/j.biotechadv.2017.12.006.
9. Soto G, Setten L, Lisi C, Maurelis C, Mozzicafreddo M, Cuccioloni M, Angeletti M, Ayub ND. 2012. Hydroxybutyrate prevents protein aggregation in the halotolerant bacterium *Pseudomonas* sp. CT13 under abiotic stress. Extremophiles 16:455–462. https://doi.org/10.1007/s00792-012-0445-0.
10. Obruca S, Sedlacek P, Mravec F, Samek O, Marova I. 2016. Evaluation of 3-hydroxybutyrate as an enzyme-protective agent against heating and oxidative damage and its potential role in stress response of poly(3-hydroxybutyrate) accumulating cells. Appl Microbiol Biotechnol 100:1365–1376. https://doi.org/10.1007/s00253-015-7162-4.
11. de Almeida A, Catone MV, Rhodius VA, Gross CA, Pettinari MJ. 2011. Unexpected stress-reducing effect of PhaP, a poly(3-hydroxybutyrate) granule-associated protein, in *Escherichia coli*. Appl Environ Microbiol 77:6622–6629. https://doi.org/10.1128/AEM.05469-11.
12. Mezzina MP, Wetzler DE, De Almeida A, Dinjaski N, Prieto MA, Pettinari MJ. 2015. A phasin with extra talents: a polyhydroxyalkanoate granule-associated protein has chaperone activity. Environ Microbiol 17:1765–1776. https://doi.org/10.1111/1462-2920.12636.
13. Mezzina MP, Pettinari MJ. 2016. Phasins, multifaceted polyhydroxyalkanoate granule-associated proteins. Appl Environ Microbiol 82:5060–5067. https://doi.org/10.1128/AEM.01161-16.
14. Bresan S, Sznajder A, Hauf W, Forchhammer K, Pfeiffer D, Jendrossek D. 2016. Polyhydroxyalkanoate (PHA) granules have no phospholipids. Sci Rep 6:26612. https://doi.org/10.1038/srep26612.
15. Jendrossek D. 2009. Polyhydroxyalkanoate granules are complex subcellular organelles (carbonosomes). J Bacteriol 191:3195–3202. https://doi.org/10.1128/JB.01723-08.
16. Bresan S, Jendrossek D. 2017. New insights into PhaM-PhaC-mediated localization of polyhydroxybutyrate granules in *Ralstonia eutropha* H16. Appl Environ Microbiol 83:e00505-17. https://doi.org/10.1128/AEM.00505-17.
17. Pfeiffer D, Jendrossek D. 2014. PhaM is the physiological activator of poly(3-hydroxybutyrate) (PHB) synthase (PhaC1) in *Ralstonia eutropha*. Appl Environ Microbiol 80:555–563. https://doi.org/10.1128/AEM.02935-13.
18. Pfeiffer D, Jendrossek D. 2012. Localization of poly(3-hydroxybutyrate) (PHB) granule-associated proteins during PHB granule formation and identification of two new phasins, PhaP6 and PhaP7, in *Ralstonia eutropha* H16. J Bacteriol 194:5909–5921. https://doi.org/10.1128/JB.00779-12.
19. Dixon R, Kahn D. 2004. Genetic regulation of biological nitrogen fixation. Nat Rev Microbiol 2:621–631. https://doi.org/10.1038/nrmicro954.
20. Udvardi M, Poole PS. 2013. Transport and metabolism in legume-rhizobia symbioses. Annu Rev Plant Biol 64:781–805. https://doi.org/10.1146/annurev-arplant-050312-120235.
21. Poole P, Ramachandran V, Terpolilli J. 2018. Rhizobia: from saprophytes to endosymbionts. Nat Rev Microbiol 16:291–303. https://doi.org/10.1038/nrmicro.2017.171.
22. Li YZ, Wang D, Feng XY, Jiao J, Chen WX, Tian CF. 2016. Genetic analysis reveals the essential role of nitrogen phosphotransferase system components in *Sinorhizobium fredii* CCBAU 45436 symbioses with soybean

and pigeonpea plants. Appl Environ Microbiol 82:1305–1315. https://doi.org/10.1128/AEM.03454-15.
23. Wang C, Saldanha M, Sheng X, Shelswell KJ, Walsh KT, Sobral BWS, Charles TC. 2007. Roles of poly-3-hydroxybutyrate (PHB) and glycogen in symbiosis of *Sinorhizobium meliloti* with *Medicago* sp. Microbiology 153:388–398. https://doi.org/10.1099/mic.0.29214-0.
24. Hu Y, Jiao J, Liu LX, Sun YW, Chen W, Sui X, Chen W, Tian CF. 2018. Evidence for phosphate starvation of rhizobia without terminal differentiation in legume nodules. Mol Plant Microbe Interact 31:1060–1068. https://doi.org/10.1094/MPMI-02-18-0031-R.
25. Yuan ZC, Zaheer R, Finan TM. 2006. Regulation and properties of PstSCAB, a high-affinity, high-velocity phosphate transport system of *Sinorhizobium meliloti*. J Bacteriol 188:1089–1102. https://doi.org/10.1128/JB.188.3.1089-1102.2006.
26. Trainer MA, Capstick D, Zachertowska A, Lam KN, Clark SRD, Charles TC. 2010. Identification and characterization of the intracellular poly-3-hydroxybutyrate depolymerase enzyme PhaZ of *Sinorhizobium meliloti*. BMC Microbiol 10:92. https://doi.org/10.1186/1471-2180-10-92.
27. Wang C, Sheng X, Equi RC, Trainer MA, Charles TC, Sobral BW. 2007. Influence of the poly-3-hydroxybutyrate (PHB) granule-associated proteins (PhaP1 and PhaP2) on PHB accumulation and symbiotic nitrogen fixation in *Sinorhizobium meliloti* Rm1021. J Bacteriol 189:9050–9056. https://doi.org/10.1128/JB.01190-07.
28. Cevallos MA, Encarnación S, Leija A, Mora Y, Mora J. 1996. Genetic and physiological characterization of a *Rhizobium etli* mutant strain unable to synthesize poly-beta-hydroxybutyrate. J Bacteriol 178:1646–1654. https://doi.org/10.1128/jb.178.6.1646-1654.1996.
29. Mandon K, Michel-Reydellet N, Encarnacio S, Kaminski PA, Leija A, Cevallos MA, Elmerich C, Mora J. 1998. Poly-β-hydroxybutyrate turnover in *Azorhizobium caulinodans* is required for growth and affects *nifA* expression. J Bacteriol 180:5070–5076.
30. Yoshida KI, Takemoto Y, Sotsuka T, Tanaka K, Takenaka S. 2013. PhaP phasins play a principal role in poly-β-hydroxybutyrate accumulation in free-living *Bradyrhizobium japonicum*. BMC Microbiol 13:290. https://doi.org/10.1186/1471-2180-13-290.
31. Quelas JI, Mesa S, Mongiardini EJ, Jendrossek D, Lodeiro AR. 2016. Regulation of polyhydroxybutyrate synthesis in the soil bacterium *Bradyrhizobium diazoefficiens*. Appl Environ Microbiol 82:4299–4308. https://doi.org/10.1128/AEM.00757-16.
32. Li Y, Tian CF, Chen WF, Wang L, Sui XH, Chen WX. 2013. High-resolution transcriptomic analyses of *Sinorhizobium* sp. NGR234 bacteroids in determinate nodules of *Vigna unguiculata* and indeterminate nodules of *Leucaena leucocephala*. PLoS One 8:e70531. https://doi.org/10.1371/journal.pone.0070531.
33. Vinardell J-M, Acosta-Jurado S, Zehner S, Göttfert M, Becker A, Baena I, Blom J, Crespo-Rivas JC, Goesmann A, Jaenicke S, Krol E, McIntosh M, Margaret I, Pérez-Montaño F, Schneiker-Bekel S, Serranía J, Szczepanowski R, Buendía A-M, Lloret J, Bonilla I, Pühler A, Ruiz-Sainz J-E, Weidner S. 2015. The *Sinorhizobium fredii* HH103 genome: a comparative analysis with *S. fredii* strains differing in their symbiotic behavior with soybean. Mol Plant-Microbe Interact 28:811–824. https://doi.org/10.1094/MPMI-12-14-0397-FI.
34. Jiao J, Ni M, Zhang B, Zhang Z, Young JPW, Chan T-F, Chen WX, Lam H-M, Tian CF. 2018. Coordinated regulation of core and accessory genes in the multipartite genome of *Sinorhizobium fredii*. PLoS Genet 14:e1007428. https://doi.org/10.1371/journal.pgen.1007428.
35. Aneja P, Zachertowska A, Charles T. 2005. Comparison of the symbiotic and competition phenotypes of *Sinorhizobium meliloti* PHB synthesis and degradation pathway mutants. Can J Microbiol 51:599–604. https://doi.org/10.1139/w05-042.
36. Vranova V, Zahradnickova H, Janous D, Skene KR, Matharu AS, Rejsek K, Formanek P. 2012. The significance of D-amino acids in soil, fate and utilization by microbes and plants: review and identification of knowledge gaps. Plant Soil 354:21–39. https://doi.org/10.1007/s11104-011-1059-5.
37. Aliashkevich A, Alvarez L, Cava F. 2018. New insights into the mechanisms and biological roles of D-amino acids in complex eco-systems. Front Microbiol 9:683. https://doi.org/10.3389/fmicb.2018.00683.
38. Reed JL, Patel TR, Chen KH, Joyce AR, Applebee MK, Herring CD, Bui OT, Knight EM, Fong SS, Palsson BO. 2006. Systems approach to refining genome annotation. Proc Natl Acad Sci U S A 103:17480–17484. https://doi.org/10.1073/pnas.0603364103.
39. Cai G, Driscoll BT, Charles TC, Cai G, Driscoll BT. 2000. Requirement for the enzymes acetoacetyl coenzyme A synthetase and poly-3-hydroxybutyrate (PHB) synthase for growth of *Sinorhizobium meliloti* on PHB cycle intermediates. J Bacteriol 182:2113–2118. https://doi.org/10.1128/JB.182.8.2113-2118.2000.
40. Knoll M, Hamm TM, Wagner F, Martinez V, Pleiss J. 2009. The PHA Depolymerase Engineering Database: a systematic analysis tool for the diverse family of polyhydroxyalkanoate (PHA) depolymerases. BMC Bioinformatics 10:89. https://doi.org/10.1186/1471-2105-10-89.
41. Handrick R, Reinhardt S, Focarete ML, Scandola M, Adamus G, Kowalczuk M, Jendrossek D. 2001. A new type of thermoalkalophilic hydrolase of *Paucimonas lemoignei* with high specificity for amorphous polyesters of short chain-length hydroxyalkanoic acids. J Biol Chem 276:36215–36224. https://doi.org/10.1074/jbc.M101106200.
42. Aneja P, Charles TC. 2005. Characterization of bdhA, encoding the enzyme D-3-hydroxybutyrate dehydrogenase, from *Sinorhizobium* sp strain NGR234. FEMS Microbiol Lett 242:87–94. https://doi.org/10.1016/j.femsle.2004.10.043.
43. Lodwig EM, Leonard M, Marroqui S, Wheeler TR, Findlay K, Downie JA, Poole PS. 2005. Role of polyhydroxybutyrate and glycogen as carbon storage compounds in pea and bean bacteroids. Mol Plant Microbe Interact 18:67–74. https://doi.org/10.1094/MPMI-18-0067.
44. Pfeiffer D, Wahl A, Jendrossek D. 2011. Identification of a multifunctional protein, PhaM, that determines number, surface to volume ratio, subcellular localization and distribution to daughter cells of poly (3-hydroxybutyrate), PHB, granules in *Ralstonia eutropha* H16. Mol Microbiol 82:936–951. https://doi.org/10.1111/j.1365-2958.2011.07869.x.
45. Mu H, Steinbu A. 2005. Influence of homologous phasins (PhaP) on PHA accumulation and regulation of their expression by the transcriptional repressor PhaR in *Ralstonia eutropha* H16. Microbiology 151:825–833.
46. Kuchta K, Chi L, Fuchs H, Pötter M, Steinbüchel A. 2007. Studies on the influence of phasins on accumulation and degradation of PHB and nanostructure of PHB granules in *Raistonia eutropha* H16. Biomacromolecules 8:657–662. https://doi.org/10.1021/bm060912e.
47. Yurgel SN, Kahn ML. 2008. A mutant GlnD nitrogen sensor protein leads to a nitrogen-fixing but ineffective *Sinorhizobium meliloti* symbiosis with alfalfa. Proc Natl Acad Sci U S A 105:18958–18963. https://doi.org/10.1073/pnas.0808048105.
48. Liu LX, Li QQ, Zhang YZ, Hu Y, Jiao J, Guo HJ, Zhang XX, Zhang B, Chen WX, Tian CF. 2017. The nitrate-reduction gene cluster components exert lineage-dependent contributions to optimization of *Sinorhizobium* symbiosis with soybeans. Environ Microbiol 19:4926–4938. https://doi.org/10.1111/1462-2920.13948.
49. Sznajder A, Pfeiffer D, Jendrossek D. 2015. Polyhydroxybutyrate (PHB) granule-associated proteins in *Ralstonia eutropha* H16. Appl Environ Microbiol 81:1847–1858. https://doi.org/10.1128/AEM.03791-14.
50. Tian CF, Zhou YJ, Zhang YM, Li QQ, Zhang YZ, Li DF, Wang S, Wang J, Gilbert LB, Li YR, Chen WX. 2012. Comparative genomics of rhizobia nodulating soybean suggests extensive recruitment of lineage-specific genes in adaptations. Proc Natl Acad Sci U S A 109:8629–8634. https://doi.org/10.1073/pnas.1120436109.
51. Remigi P, Zhu J, Young JPW, Masson-Boivin C. 2016. Symbiosis within symbiosis: evolving nitrogen-fixing legume symbionts. Trends Microbiol 24:63–75. https://doi.org/10.1016/j.tim.2015.10.007.
52. Capela D, Marchetti M, Clérissi C, Perrier A, Guetta D, Gris C, Valls M, Jauneau A, Cruveiller S, Rocha EPC, Masson-Boivin C. 2017. Recruitment of a lineage-specific virulence regulatory pathway promotes intracellular infection by a plant pathogen experimentally evolved into a legume symbiont. Mol Biol Evol 34:2503–2521. https://doi.org/10.1093/molbev/msx165.
53. Pueppke SG, Broughton WJ. 1999. *Rhizobium* sp. strain NGR234 and *R. fredii* USDA257 share exceptionally broad, nested host ranges. Mol Plant Microbe Interact 12:293–318. https://doi.org/10.1094/MPMI.1999.12.4.293.
54. Quandt J, Hynes MF. 1993. Versatile suicide vectors which allow direct selection for gene replacement in Gram-negative bacteria. Gene 127:15–21. https://doi.org/10.1016/0378-1119(93)90611-6.
55. Ditta G, Stanfield S, Corbin D, Helinski DR. 1980. Broad host range DNA cloning system for Gram-negative bacteria: construction of a gene bank of *Rhizobium meliloti*. Proc Natl Acad Sci U S A 77:7347–7351. https://doi.org/10.1073/pnas.77.12.7347.
56. Oke V, Long SR. 1999. Bacterial genes induced within the nodule during the *Rhizobium*-legume symbiosis. Mol Microbiol 32:837–849. https://doi.org/10.1046/j.1365-2958.1999.01402.x.
57. Marx CJ, Lidstrom ME. 2002. Broad-host-range *cre-lox* system for antibiotic marker recycling in gram-negative bacteria. Biotechniques 33:1062–1067. https://doi.org/10.2144/02335rr01.

58. Kovach ME, Elzer PH, Hill DS, Robertson GT, Farris MA, Roop RM, II, Peterson KM. 1995. Four new derivatives of the broad-host-range cloning vector pBBR1MCS, carrying different antibiotic-resistance cassettes. Gene 166:175–176. https://doi.org/10.1016/0378-1119(95)00584-1.
59. Vincent JM. 1970. A manual for the practical study of root nodule bacteria. Blackwell Scientific, London, United Kingdom.
60. Ling Q, Huang W, Jarvis P. 2011. Use of a SPAD-502 meter to measure leaf chlorophyll concentration in *Arabidopsis thaliana*. Photosynth Res 107:209–214. https://doi.org/10.1007/s11120-010-9606-0.
61. Van de Velde W, Guerra JCP, de Keyser A, de Rycke R, Rombauts S, Maunoury N, Mergaert P, Kondorosi E, Holsters M, Goormachtig S. 2006. Aging in legume symbiosis. A molecular view on nodule senescence in *Medicago truncatula*. Plant Physiol 141:711–720. https://doi.org/10.1104/pp.106.078691.
62. Spiekermann P, Rehm BHA, Kalscheuer R, Baumeister D, Steinbüchel A. 1999. A sensitive, viable-colony staining method using Nile red for direct screening of bacteria that accumulate polyhydroxyalkanoic acids and other lipid storage compounds. Arch Microbiol 171:73–80. https://doi.org/10.1007/s002030050681.
63. Preusting H, Kingma J, Huisman G, Steinbüchel A, Witholt B. 1993. Formation of polyester blends by a recombinant strain of *Pseudomonas oleovorans*: different poly(3-hydroxyalkanoates) are stored in separate granules. J Environ Polym Degrad 1:11–21. https://doi.org/10.1007/BF01457649.
64. Ishihama Y, Oda Y, Tabata T, Sato T, Nagasu T, Rappsilber J, Mann M. 2005. Exponentially modified protein abundance index (emPAI) for estimation of absolute protein amount in proteomics by the number of sequenced peptides per protein. Mol Cell Proteomics 4:1265–1272. https://doi.org/10.1074/mcp.M500061-MCP200.
65. Law JH, Slepecky RA, Law JH, Slepecky RA. 1961. Assay of poly-β-hydroxybutyric acid. J Bacteriol 82:33–36.
66. Quelas JI, Mongiardini EJ, Pérez-Giménez J, Parisi G, Lodeiro AR. 2013. Analysis of two polyhydroxyalkanoate synthases in *Bradyrhizobium japonicum* USDA 110. J Bacteriol 195:3145–3155. https://doi.org/10.1128/JB.02203-12.